Eva Gleichweit, BSc

UV/Ozone Surface Treatment for Bonding of Elastomeric COC-Based Microfluidic Devices for Medical Application

MASTER'S THESIS

to achieve the university degree of

Diplom-Ingenieurin

Master's degree programme: Biomedical Engineering

submitted to

Graz University of Technology

Supervisor

Univ.-Prof. Dipl.-Ing. Dr.techn. Christian Baumgartner

Institute of Health Care Engineering

Dipl.-Ing. Dr. Stefan Köstler, Erba Technologies Austria GmbH

Graz, September 2018

AFFIDAVIT

I declare that I have authored this thesis independently, that I have not used other than the declared sources/resources, and that I have explicitly indicated all material which has been quoted either literally or by content from the sources used. The text document uploaded to TUGRAZonline is identical to the present master‘s thesis.

Date

Signature

Acknowledgments

At this point, I would like to thank all those who have supported and motivated me during the time I worked on this thesis.

First of all a special thank you to Stefan Köstler, who supported me during my intership at Payer Medical GmbH for 6 months and beyond. He had always an open door for my concerns and always knew a way out of a dead end.

I am very thankful for the support of my supervisor Prof. Baumgartner, who responded very quickly to my mails and had always time for appointments and feedback. I think such a concession is not self-evident and I appreciated it very much.

Special thanks go to my fellow students and friends, whose suggestions have continuoulsy improved my work. They sacrificed a lot of time and effort and I am very grateful for that.

I specially thank my life partner Christian for the strong emotional support and motivation over the duration of my entire studies. You gave me the motivation I needed.

To thank my family, I switch to german.
Abschließend würde ich gerne meiner Familie danken, die immer an mich geglaubt und mir das Studium durch großartige Unterstützung ermöglicht hat.

Abstract

Reliable bonding of microstructured polymer parts is one of the major challenges in industrial fabrication of microfluidic devices. In the present thesis, the effects of a UV/ozone surface activation on the bonding process were investigated for the combination of a commonly used thermoplastic cyclic olefin copolymer (COC) with an elastomeric COC (eCOC) as a new thermoplastic elastomer material. Bonding was studied using two-component injection molded parts of COC and eCOC, along with microfluidic COC chips. Chemical modification of the polymer surfaces by UV/ozone treatment was investigated by using ATR-IR Spectroscopy and contact angle measurements. For both materials, carbonyl peaks appeared in the infrared spectra and a marked contact angle decrease was found, in particular during the first 10 min of UV/ozone exposure. Subsequently, thermocompression bonding was investigated systematically using variation of temperature and pressure holding time in a design-of-experiment approach. Surface activation and bonding process parameters were optimized and bond strengths were characterized by the wedge test method. The results showed that strong bonding of this polymer materials combination can be achieved at temperatures significantly below the bulk glass transition temperature of COC.

Contents

List of Figures

List of Tables

Table of Abbreviations

Chapter 1

Introduction

Over the last decades, the use of microfluidic devices have become more popular due to several significant developments and resulting advantages. Compared to typical bulky laboratory equipment, advantages such as low consumption of chemicals, biocompatibility, low costs, and the fast analysis of samples make them appealing. Beside the functional advantages, the small size of the devices makes them portable and practicable in use. The application area is broad, ranging from biology, chemistry and engineering to medicine and pharmaceuticals. Especially for medical applications, microfluidics offer an interesting field in terms of point-of-care-testing (POCT) and micro total analysis system (µTAS), where laboratory diagnosis could be done directly on the infirmary or the steps of analyzing are totally automated like a lab-on-a-chip. In Austria, the healthcare system is relatively extensive, well established and accessible for everyone. Nevertheless, medicine, including diagnostics and therapy, is a continuously developing area and patient near and especially fast diagnostic analysis are important aspects to consider in case of research activities. In developing countries, where reliable electricity, infrastructure, costs of reagents, and longtime processes still play a tremendous role, POCT or µTAS are significant fields to ensure medical treatment. [1, 2]
In the beginning of the development of microfluidics, the processed materials were glass and silicone. However, due to high costs of the raw materials and manufacturing processes, alternative materials were continuously sought after. In contrast to glass and silicone, thermoplastic polymers show physical advantages like optical behavior and chemical resistance. In addition, when considering the economic aspect,

the lower price makes the polymer-family appealing for microfluidic devices. The most commonly used thermoplastic polymers are described in Section 2.2. [1, 2]
Moreover, an important aspect of the industrial fabrication of thermoplastic polymers is reliable bonding of the polymer parts. There are requirements to fulfill in order to ensure a proper, tight sealing without clogging or changing the channel geometries. Section 2.4 describes several so-called bonding procedures or technologies to seal microchannels. [2, 3]

1.1 Aim of the Thesis

The bonding process is still one of the key issues in industrial fabrication of thermoplastic microfluidic devices. In particular, for microvalves and other actuators requiring the combination of elastomeric and rigid polymer materials, reliable bonding is a major challenge. Several different thermocompression bonding methods with additional surface activation by, e.g., solvents, plasma, UV, corona and etc., have been described. [4]
In this thesis, bonding of a new material combination, consisting of microstructured cyclic olefin copolymer (COC) parts with a novel thermoplastic elastomer material, called elastomer cyclic olefin copolymer (eCOC), applied as two-component injection molded cover parts was investigated.
The aim of this thesis is to give an overview of the current bonding technologies for thermoplastic polymers and to point out surface modifications for thermocompression bonding at lower temperatures. A special focus is set on the chemical modification of the surface due to ultraviolet radiation. After UV/ozone activation, the material surfaces were investigated and the subsequent thermocompression bonding process was evaluated. Studies have shown that the application of UV/ozone surface modification has positive effects on the bonding qualities. Based on these findings, the hypothesis that lower bonding temperatures and shorter bonding times are required by applying UV/ozone surface activation on the new material combination was investigated.

Chapter 2

Fundamentals

In the beginning of the 20^{th} century, terms like µTAS and lab-on-a-chip appeared, indicating the launch of microfluidic devices. While glass and silicone were dominating materials for early microfluidic devices, polymers became more popular for the fabrication of medical devices during the 1960s. There are two main reasons why the trend drifted away from glass and silicone towards plastics. The first being due to the costs of the raw materials, the granular plastics, and fabrication processes, which are lower than for glass or silicone. Secondly, that plastic is much easier moldable compared to glass and silicone. Polymers are used in medical engineering as packing material, for medical devices, disposables and implants with different requirements according to their application. [5, 6]

The subsequent sections are structured in a way the reader can follow the development process of a polymer microfluidic device. First, some basics on microfluidics and their application is presented, followed by different polymer materials that are most commonly used. The next step in a microfluidic development process is the fabrication technique. To seal the microchannels in a fourth step, different bonding technologies and their advantages and disadvantages are shown, with a special focus on UV/ozone bonding. The end of the chapter points out the different methods for quantifying the bond strength and the surface properties after the UV/ozone exposure of a polymer.

2.1 Microfluidics

In general, one speaks of microfluidics at channel width from 1 µm to 1 mm. The geometries, the lengths of the channels and the size of the polymer plate vary depending on the application of the device. In practical applications, the channel widths vary most commonly between 50 µm and 500 µm. The lengths range between a few millimeters to centimeters. Because of the small channels and the resulting small amount of fluid, there are other dominant effects than in case of a macrofluidic system. In macrofluidic systems, volume-linked effects like gravity and inertia have significant impact on the system. In case of a microfluidic system, these effects are negligible. Because of the high ratio between amount of fluid and the surface of the channel, effects like interfacial tension, electrostatic and electrokinetic forces are dominant. Therefore, the design of a microfluidic device is challenging and interdisciplinary. [2, 3]
One possible application of microfluidic devices is synthesizing oligonucleotides, which are oligomers that are made of several nucleotides. Oligomers are molecules which consist of structurally identical or similar units. Nucleotides are building blocks of nucleic acids and are made of three components. First is the base, which is one of five possible nucleobases (adenine, guanine, cytosine, thymine or uracil). The second component is sugar (monosaccharide), whereas the third component is phosphate. In Section 3.1, the microfluidic polymer part for synthesizing oligonucleotides as primer for DNA amplification is presented. The synthesis can be done by a solid-phase synthesis, which was invented in the 1960s by Bruce Merrifield [7]. Solid supports are needed for this synthesis method, where the oligonucleotides are bonded. For these small supports, typically 50 µm - 200 µm in diameter, controlled pore glass and Polystyrene (PS) are mostly used.
The orientation of a DNA strand is described by the location of the bonded phosphate group of the next nucleobase, which is located on 3'. The synthesis proceeds in the 3'- to 5'-direction, where typical biosynthesis works directly in the opposite direction, in 5'- to 3'direction. During one synthesis cycle, there is one nucleotide added, see Figure 2.1.

For more detailed information about the synthesis cycle the interested reader is refered to [7].

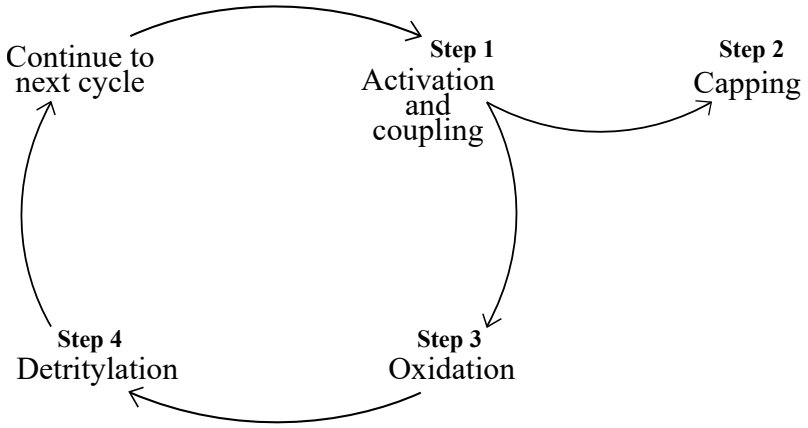

Figure 2.1: Schematic of oligonucleotide synthesis cycle, modified from [7].

2.2 Thermoplastic Polymers

Especially for medical applications, the type of material used for microfluidic devices is important due to biocompatibility and high requirements. Thermoplastics and Polydimethylsiloxane (PDMS) are the most commonly used materials in microfluidic applications. A polymer is made of single chains, several so-called monomer units, which are low molecular and highly reactive molecules. They can bind together to macromolecules, and depending on the way they react with each other, one distinguishes between polycondensation, polyaddition and polymerization. Due to the different monomer binding combinations, specific physical characteristics are settled, like the glass transition temperature (T_g) and the melting temperature (T_m). [6, 8] All polymers are in a glasslike behavior, at very low temperatures. The border of this behavior is depending on the composition of the polymer chain. For this state, the molecular movements of the main chain are frozen and the polymer becomes brittle. The T_g describes the temperature at which the change of the brittle property to ductile behavior occurs. Based on their behavior, polymers can be divided into thermoplastics, elastomers and duroplasts as shown in Figure 2.3.

By changing the temperature of thermoplastics, the different viscour, rubber and glass-like polymer states can be seen. For applications in the field of microfluidics and the fabrication of microfluidic devices, the change in the behavior from glass-like to viscous is beneficial, because it makes them precisely moldable. Another special property of thermoplastics is the possibility of being reheated several times without changing any of their characteristics. Only due to overheating, the material starts

to decompose thermally.

Thermoplastics can be amorphous or semi-crystalline. Amorphous means that the atoms of the material are not structured, i.e., form an irregular pattern, while crystalline materials show three-dimensional and periodically organized structures. However, semi-crystalline thermoplastics have both, amorphous and crystalline components in the structure, as can be seen in Figure 2.2. The semi-crystalline structure of thermoplastics gives them a high strength compared to amorphous ones, even above the T_g. Amorphous thermoplastics are therefore only used below T_g. Semi-crystalline thermoplastics are used just before the viscous state of the polymer. Figure 2.3 lists examples of amorphous and semi-crystalline thermoplastics. [8, 9]

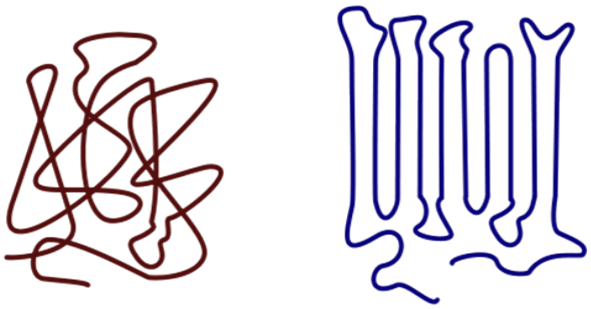

Figure 2.2: Structure of amorphous (left) and semi-crystalline (right) thermoplastics, taken from [10].

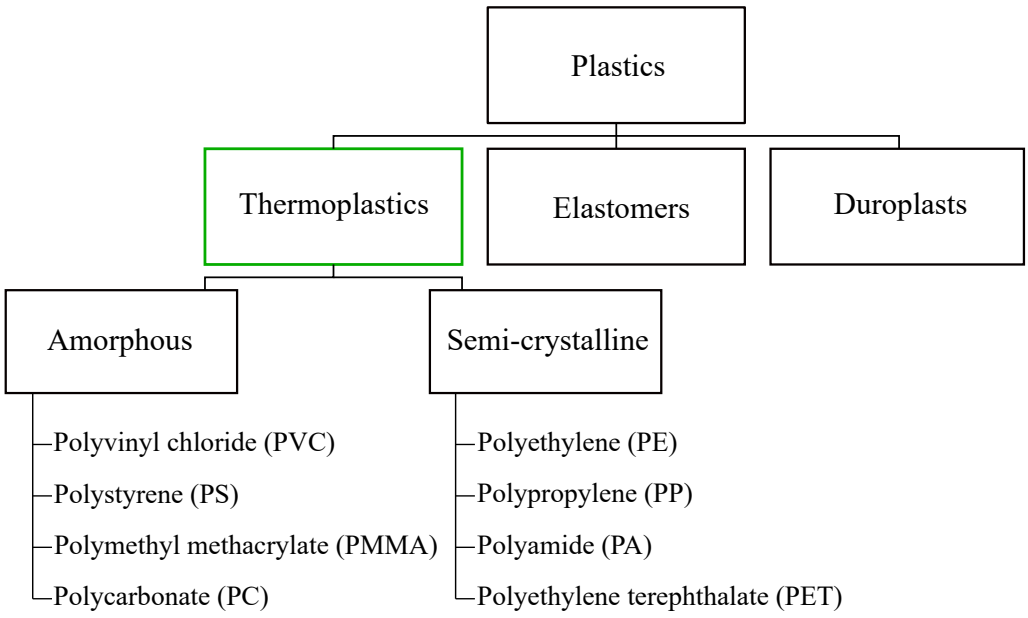

Figure 2.3: Classification of plastics, modified from [9].

The T_g of elastomers is lower than room temperature. They are elastic deformable and show the typical rubber-like behavior above the T_g. For temperatures below T_g, they may loose their typical behavior. Elastomers do not melt due to the chemical crosslinking making it difficult to reuse them.
PDMS is a frequently used elastomer in microfluidic applications. A hybrid material of thermoplastics and elastomers are called thermoplastic elastomers. At room temperature, they show a similar behavior to elastomers but when heated they are deformable and show thermoplastic properties. Copolymers often show this behavior.
Duroplasts are highly crosslinked polymers which are not deformable after they have hardened. The temperature of decomposing is often lower than the T_g with the consequence that duroplasts show no softening behavior and are not reusable. The Young's modulus describes the stiffness of a solid material, and lies between 600 MPa and 4000 MPa for thermoplasts and duroplasts, while for elastomers it is reported to be between 50 MPa and 600 MPa. [8, 9]

There are many polymeric materials used for microfluidic applications. This thesis focuses on the most commonly used thermoplastic polymers, which all have an amorphous structure. Therefore, a more detailed explanation of available amorphous thermoplastics is described subsequently.

2.2.1 Polystyrene

The starting products for styrene are two primary chemicals, which are extracted from petroleum, benzene and ethylene. In the presence of zeolites they are compounded to ethylbenzene, after which styrene and hydrogen result by heat induction. Therefore, the main chain of Polystyrene (PS) consists of hydrocarbon compounds, as is the case for Polyethylene (PE) or Polypropylene (PP). The differences between PE, PP and PS are the functional side groups, which lead to different physical properties. The side group of PS is the benzene ring ($-C_6H_5$), as can be seen in Figure 2.4. Therefore, the T_g is 100 °C and the T_m is reported to be 270 °C. Typical manufacturing processes of PS are continuous bulk polymerization and suspension polymerization. Furthermore, PS is a nonpolar and soluble polymer. [8, 9]

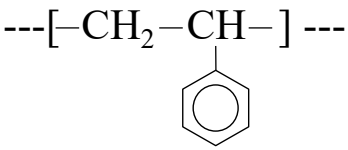

Figure 2.4: Structural formula of PS, showing the main chain with a benzene ring as side group, modified from [9].

2.2.2 Polycarbonate

Every polycondensate containing a group of ester belongs to the group of thermoplastic polyester. The most popular is the Polycarbonate (PC), which is a thermoplastic polyester of carbonic acid with aliphatic or aromatic dihydroxy-components. Polycarbonates are mainly amorphous and have a high strength, low water absorption and are transparent. The T_g of PC is about 145 ℃ . PC is polar and soluble. For medical applications PC is mainly used for manufacturing syringes and tubes. Figure 2.5 shows the structural formula of Bisphenol-A-Polycarbonate. [5, 11, 9]

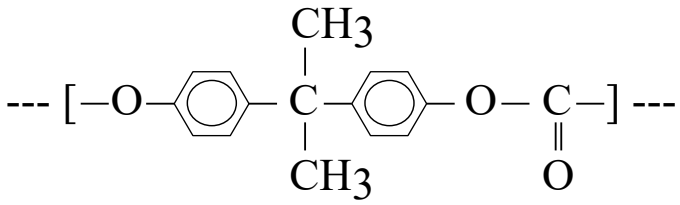

Figure 2.5: Structural formula of Bisphenol-A-Polycarbonate with two phenol-groups between the oxygen atoms, modified from [9].

2.2.3 Polymethyl Methacrylate

Since 1933, Polymethyl methacrylate (PMMA) is better known as acrylic glass (Plexiglas®). The material shows good mechanical and chemical properties such as a high stiffness and hardness, as well as good resistance to weak acids, bases and nonpolar solvents. Therefore, PMMA is an often used material for microfluidic devices. Starting products of PMMA are acetone, obtained from the petroleum via propylene, and by burning a mixture of gas and ammonia at the platinum contact produced hydrocyanic acid. PMMA can be produced by various of radical polymerization of methyl esters of methacrylic acids. The T_g is about 115 ℃. PMMA is polar and soluble. Figure 2.6 shows the structural formula of PMMA. [9, 11]

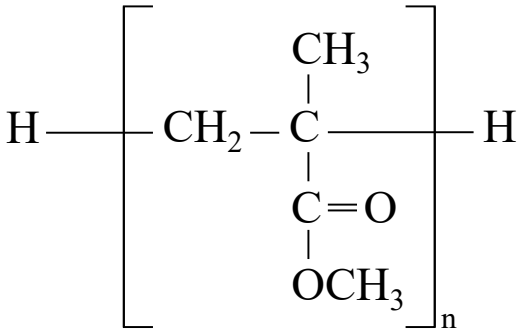

Figure 2.6: Structural formula of PMMA, where n implies the possible variation in the length of the polymer chain, modified from [12].

2.2.4 Cyclo Olefin Copolymer

Cyclic olefin polymer (COP) is based on cyclic olefin monomers and ethene. If there is more than one type of monomer, it is called cyclic olefin copolymer (COC). In general, COC exhibits a lower water absorbance than PC, a high resistance against acids and polar solvents, as well as a high strength and rigidity. Furthermore, COP displays physical advantageous properties due to its high optical transparency. Another aspect is its thermal behavior, where COC is available with different glass transition temperatures, making it an attractive material for microfluidic applications. A negative aspect of COC is its hydrophobicity. The untreated material shows contact angles of de-ionized (DI) water at about 90 °. The COC is nonpolar and has an amorphous structure which leads back to the trade name Topas® which stands for Thermoplastic Olefin Polymers of Amorphous Structure. Figure 2.7 shows a part of the structural formula of COC. [9, 13]

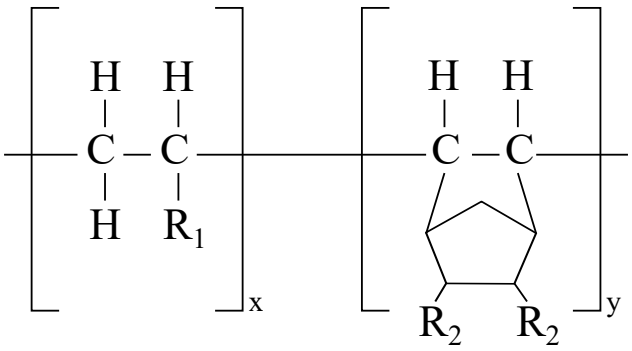

Figure 2.7: Part of the structural formula of COC, where x and y imply the possible variation in the length of the polymer chain, modified from [9].

2.3 Fabrication Methods

After the design of a microfluidic device and the selection of the material, the choice of fabrication method becomes the next important issue. Wu *et al.* [11] divided the microfabrication methods in photolithography-based and replication based methods. The most suitable fabrication method depends on several factors, like substrate, costs, time, or size of the device. For photolithography methods, a photosensitive material is defined by using light. Depending on the wavelength of the light, different aspect ratios of the channels can be achieved. For replication-based methods, a mold is necessary, which can be fabricated by photolithography or mechanical tools. It gives the substrate its shape without deforming during the fabrication process. [11, 14]
Researchers often use rapid prototyping methods, like computer numerical controlled (CNC) milling, or laser ablation for feasibility studies of their microfluidic devices. For mass production, the rapid prototyping methods are too expensive and time consuming and therefore, replication and photolithography-based methods are mainly used. [6]
In general, there is no fabrication method deemed as the best choice for microfluidic devices. Subsequently, the most commonly used fabrication methods for polymer microfluidic devices are summarized. [6]

2.3.1 Photolithography

The principle of this method is patterning a photosensitive material by exposing it to light. By using a mask, the exposed parts can be defined, by which their behavior changes due to specific properties of the photosensitive material and wavelength of the emitted light. Afterwards, the irradiated or the unirradiated parts, depending on the photo resist, can be cleared off. Photolithography is often used for the fabrication of the master molds for replication-based fabrication methods. Principally, the process is well established, but has two significant disadvantages. Firstly, the costs of the materials are high, whereas the second disadvantage is the necessity of a clean room. [11, 14]

2.3.2 Hot Embossing

Hot embossing is a relatively simple way to fabricate structured polymer devices and it was a common technique even before microfluidic devices were of interest. The polymer becomes moldable after heating it above the T_g. The mold is then pressed onto the polymer like a stamp which results in forming the negative structure into the polymer, as it is shown in Figure 2.8. However, hot embossing is limited for thermoplastic polymers because of its ability to change their behavior from glass-like to viscous and vice versa by applying heat. This technique is easily implemented in an ordinary heat press and is often used in a laboratory environment for manufacturing microfluidic devices. Another variant of hot embossing is roll-to-roll embossing. Instead of a fixed stamp, the mold and the polymer are pressed together between two rolls and are rotated to transfer the structures of the mold onto the polymer. The roll is heated for changing the glass-like behavior of the polymer to a viscous state. Instead of simple hot embossing, the roll-to-roll method is a continuous fabrication method and ensures a high throughput. The possibility to combine roll-to-roll embossing with bonding technologies in industrial facilities is another advantage of roll-to-roll embossing. [11, 15]

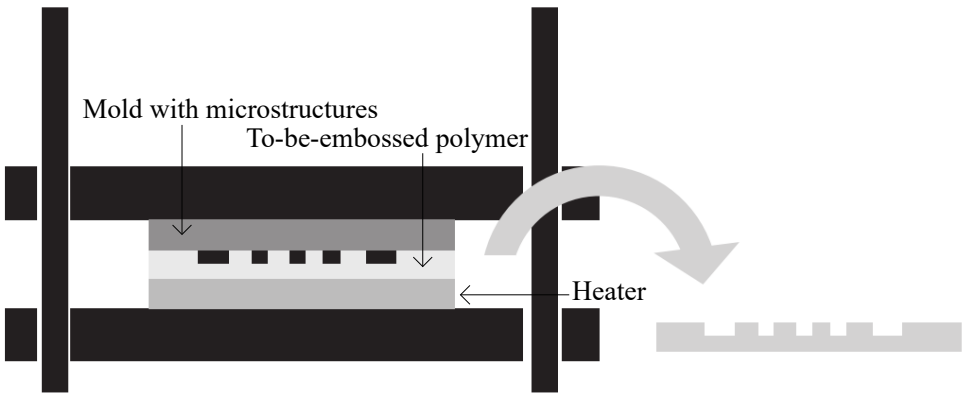

Figure 2.8: Schematic of hot embossing, modified from [11].

2.3.3 Soft-Lithography

Soft-lithography is one of the main manufacturing processes for microfluidic structures. It is a relatively simple and low cost replication-based process, where a mold

is necessary to form the required structures. The polymer takes form by applying it onto the mold. After the application, the polymer is cured by temperature or by UV radiation and is then peeled off the mold. In the case of molding an elastomer, it gets directly mixed with a curing agent. [11]

2.3.4 Injection Molding

For mass production of microfluidic devices, injection molding is a popular fabrication method, because of the short processing time. However, disadvantages of this method are the high acquisition costs and the monetary investment that has to be made for the special mold before the first new device can be manufactured. [15]
Injection molding is a very advanced technology to fabricate polymer devices. A solid granular plastic is melted, shaped in form by high pressures, cooled, followed by the ejection of the finished device from the machine. Figure 2.9 shows a schematic representation of an injection molding device.

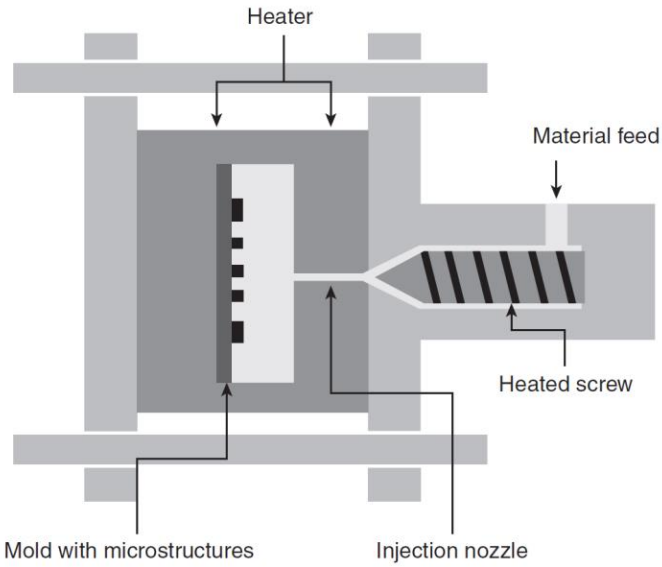

Figure 2.9: Schematic of injection molding, taken from [11].

The steps of the process for injection molding are [5]:

1. Plasticizing and metering
2. Injection, holding pressure and cooling
3. Ejection of the parts

This process is fully automated and can produce parts with complex geometries and with weights ranging from a few milligrams to several kilograms. The time of a production cycle varies depending on the manufactured device, but lies in between one second and about 10 minutes. This technique uses the physical properties of thermoplastics for melting, forming, and cooling the material. [5, 16]

1. Plasticizing and metering
The dried raw material reaches the plasticizing tool via a funnel. However, some machines have a dryer instead of the funnel in order to dry the raw material according to manufacturer's specifications. Afterwards, it reaches the plunger. Because of its screw-like shape the granular plastic is transported to the mold by the rotating plunger and is melted due to shear forces and heat transfer from the cylindrical wall to the substrate. At the tip of the plunger, plasticized material is accumulated until the adjusted metering way is finished. The rotation of the plunger is stopped when the desired volume is accumulated. The volume is determined by the cavity of the mold and the shrinkage volume when the material is cooled. [5, 16]

2. Injection, holding pressure and cooling
During injection, the mold needs to be closed to make sure the plasticized polymer fills the entire mold. This is necessary for the accumulation of the plasticized polymer. The plunger is pushed towards the nozzle to fill the mold with the plasticized polymer. Thereby, the plunger is not rotating anymore. A barrier ensures that the melted polymer is not able to flow back into the plunger. During the phase of holding pressure, the polymer inside the mold gets compressed in order to compensate the loss of volume due to cooling. This pressure is active until the sprue is hardened. To ensure a reliable stiffness for the ejection of the device, a residual cooling time is used. During this cooling time the metering process starts again for the next part. [5, 16]

3. Ejection of the parts
After the cooling process has finished, the parts can be removed either by a hydraulic, electro-mechanic or pneumatic ejection mechanism. After the mold is closed, the injection process starts again. [5, 16]

A special form of injection molding is the multi-component injection molding, which allows to produce parts that consist of more than one polymer. Due to this tech-

nique, it is possible to create different functionalities during one manufacturing step. For example, a sealing ring can be injection molded as a second component. [5]
In case of the microfluidic device for the Kilobaser presented in Section 3.1, the membrane plate is injection molded of two components, COC and eCOC.

2.4 Bonding Technologies

The last step of fabricating a polymeric microfluidic device is the sealing of the channels. Therefore, the bonding process sets the characteristics of the final device, like bond strength, functionality, optical and geometrical characteristics. It can show some difficulties and it is necessary to choose the most appropriate process for each application to fulfill the requirements. Riegger *et al.* [17] summed up the parameters which influence the bonding process and therefore have to be considered. To find the most suitable bonding procedure, the design of the microfluidic chip has to be studied, because it has a major influence on the bonding process. If there are small and shallow channels, the development of the bonding process is much more difficult than for large and deep channels, because the risk of clogging is reduced, see Table 2.1. Other influencing parameters are, for example, surface planarity and activation. The parameter with the most influence on the bonding process may vary depending on the chosen bonding technology, because each of them possess other difficulties. [17]

Table 2.1: Effect of channel geometries on the development of the bonding process [17].

Bonding process development	**Channel geometries**	
Little effort	Large	$>$ 1 mm
	Deep	$>$ 500 µm
Great expense	Small	$\leq$ 500 µm
	Shallow	$\leq$ 200 µm

Table 2.2 summarizes several different bonding technologies used to seal the microfluidic channels. According to literature, the technologies can be divided in direct and indirect, or direct and intermediate bonding techniques. Direct bonding means that

no intermediate bonding material is necessary. Typical direct bonding techniques are ultrasonic welding or thermal bonding. Indirect, or intermediate bonding, means that an intermediate bonding material is required to seal the channels. A typical example of an indirect bonding technique is adhesive bonding. [4, 6, 18]

Table 2.2: Possible bonding technologies.

Thermal bonding	Solvent assisted bonding
	UV/ozone assisted bonding
	Plasma assisted bonding
Ultrasonic welding	
Laser welding	Contour welding
	Mask welding
Adhesive bonding	Adhesive sticky tape application
	UV-curing adhesives
	Thermally curing adhesives
Mechanical joining	Screwing
	Clamping
	Hot/cold caulking
In-mold bonding	

The challenge of bonding microfluidic devices is the low surface energy of thermoplastic polymers, which leads to hydrophobic surfaces and lower bond strengths. The goal is to increase the surface energy for an enhanced wettability, resulting in higher bond strength of the microfluidic devices. Tsao *et al.* [4] explained that this can be achieved '[...]from either molecular entanglement or charge interactions' [4]. Thermal bonding for example is a process based on entanglement by mechanical coupling due to diffusion between the surfaces. Charge interactions arise during adhesive bonding techniques [19]. Further, Tsao *et al.* described:

> *'[...]bonding due to charge interactions can result from electrostatic or chemical (covalent) bonding, acid-base interactions, or van der Waals forces' [4].*

The possibility of bonding dissimilar materials paves the way for special building blocks of microfluidic devices, the valves. Valves have the ability to regulate flows or the addition of fluids in a microfluidic system. Different mechanisms are used to activate the valves like pneumatic, thermal or with the support of electricity. To manufacture a valve, it is necessary to bond different layers of polymer. The major technique is bonding three layers of the elastomer PDMS. Gu *et al.* [20] described two combinations of dissimilar materials, both times thermoplastic polymers bonded with PDMS. The group showed that bonding of COC and PDMS is possible and with optimized bonding parameter, a high bond strength can be achieved. Furthermore, they successfully bonded PMMA and PDMS. Due to the lower T_g of PMMA the group determined lower bonding temperatures compared to COC/PDMS.
Ogilvie *et al.* [21] bonded Viton® membrane, a special elastomer, instead of PDMS, with COC and PMMA. They realized pneumatic microvalves on PMMA and COC substrates. The modification prior to thermal bonding was done with oxygen plasma treatment, as described in Section 2.4.1.1.
Another example for bonding one stiff polymer with a flexible membrane or elastomer is the research of Herrlich *et al.* [22]. This group realised a drug delivery device by solvent bonding a flexible membrane on an injection molded COC housing. The option of bonding two different materials for manufacturing valves or similar building blocks in micofluidic devices allows a broad application area due to advantageous functionalities and possibilities.

Below, a summary of the most frequently used direct and intermediate bonding technologies including their advantages and disadvantages are presented.

2.4.1 Direct Bonding Technologies

2.4.1.1 Thermal Bonding

Thermal bonding is the most common bonding technique, because of several reasons. First of all, the process itself is cost efficient and easy to realize. For thermal bonding, the substrates are heated and pressed together to achieve a uniform contact and an optimal distribution of heat on the bonding interface. The temperature is set near the T_g of the substrate and in combination with the applied pressure, the requirements for a fusion of the polymer chains are fulfilled and a strong bond is

possible. The resulting bond strength can exceed the cohesive strength of the bulk material if the circumstances are ideal. Another advantage is the relatively easy implementation since only a hot press is needed. The fact that thermal bonding is a direct bonding technology is benefitial, too. Therefore, no intermediate or assisting material is necessary to realize good bonding qualities with high bond strengths. This indicates that the channels have homogeneous surface properties when the same material is used for the bonding parts. A big challenge in thermal bonding is the risk of deformed channels due to non-optimized temperatures. It is important to find the optimal temperature to achieve high bond strengths without destroying the channel geometries or clogging them with molten polymer. It is necessary to control the bonding parameters, like temperature, time and pressure to find the best compromise between bond strength and channel deformation. According to literature, there are different devices used to realize thermal bonding, like a programmable hot press, probably the best choice, or a roller laminator. Thermal bonding has been used for several different polymers like PC, COC or PS and also for bonding two different materials. For two different glass transition temperatures, it is easier to find the right temperature, because only one material softens and the risk of deforming the channels is lower. In general, the bond strength is high if the bonding temperature is higher than the Tg, because the polymer chains are connected. Nevertheless, the higher the temperature, the more the channels suffer and deform or collapse. There are some assisting effects to improve the bond strength and decrease the temperature to aviod this drawback. [4, 18]

Solvent Assisted Bonding

A possibility to increase the bond strength is the assistance of solvents. Due to polymer solubility, the polymeric chains link better to each other, because they become more mobile across the interface. The solubility parameter δ, also called the Hildebrand parameter, describes the interaction between the solvent and the polymer. If δ of the polymer and the solvent is very similar, dissolution can happen. δ is defined as the square root of the cohesive energy density (CED),

$$\delta = \sqrt{(CED)} = \sqrt{\frac{\Delta E_V}{V}} \quad , \tag{2.1}$$

where ΔE_V is the cohesive energy and V is the molar volume. Cohesive energy is a measure to describe the cohesive properties of a polymer. Cohesive bonds

are mostly hydrogen bonds for organic materials, van der Waals forces, or dipole-dipole interactions. By dividing the cohesive energy by the molar volume, the CED is obtained. In Table 2.3, the Hildebrand parameters for polymers and organic solvents, as mentioned in Section 2.2, are summarized. [4, 13, 23]

Table 2.3: Solubility parameters for thermoplastics and solvents [4].

Thermoplastics	δ in $(J/cm^3)^{1/2}$
PS	18.7
PC	19.4
PMMA	20.1
COC	17.7
Solvents	δ
Acetone	20.4
Isopropanol	23.4
Methylene dichloride	19.8
Cyclohexane	16.7
Water	47.7

In general, there are two different methods to expose the polymer to the solvent, either in liquid or vapor phase. For performing surface modification by bringing the solvent on the polymer in liquid phase, it is necessary to choose a solvent with dissimilar Hildebrand parameters. Otherwise, the solvent may cause a channel deformation. Beside the Hildebrand parameter, the exposure time to the solvent plays a tremendous role. If it is too long, it may change the channel geometries. Therefore, the exposure time has to be reduced for similar Hildebrand parameters, like for the combination of PMMA and acetone as a solvent. [4]

The liquid solvent can be applied on the polymer surface with a pipette or a dispensing tool. Another challenge with respect to the liquid phase is the high volatility of the solvent. Wan *et al.* [24] presented a solution for this problem by fabricating so called retention grooves to limit the evaporation of the solvent on the polymer surface.

Ogilvie *et al.* [21] and Ogończyk *et al.* [25] demonstrated a solvent treatment by vapor phase. The experimental setups are different like Ogilivie *et al.* [21] positioned

the polymer substrate on glass stand offs in a petri dish filled with the solvent and closed it with a lid. They showed that the surface roughness decreased significantly after the optimal exposure time of 4 minutes. The latter group built an experimental setup including a desiccator, with the polymer substrate enclosed, connected to a flask containing the solvent. They used magnetic stirrers to ensure homogeneity in the desiccator and showed that it is a big advantage to modify the surface by a solvent. Therefore, they were able to reach reliable bonds for temperatures below the glass transition. [21, 25]

Plasma Assisted Bonding

Another method to modify the surface prior to thermal bonding is the pretreatment by plasma. The chemical reactions at the surface depend on the polymer, plasma gas, plasma pressure, plasma power, as well as the treatment time. Roy *et al.* [26] used a low pressure plasma source and two different gases for plasma generation, argon and oxygen. As for UV/ozone pretreatment, the radicals formed during plasma exposure induce the surface to be more hydrophilic. Van Midwoud *et al.* [27] detemined the hydrophobic recovery for up to 4 weeks after the treatment by oxygen-plasma. They examined different polymers, including COC. For COC a faster increase of the contact angles after one week is detectable, compared to the results after one week of UV/ozone treatment. Therefore, the group concluded a preference of UV/ozone pretreatment. Apart from this, the experimental setup for plasma exposure is more expensive compared to UV/ozone. [26, 28]

UV/Ozone Assisted Bonding

The last method presented in this thesis to modify the surface of a polymer microfluidic device is the pretreatment by UV radiation. In 1972, the first intention of using UV/ozone was to clean the surfaces of semiconductor substrates from organic contaminants. [19, 29]

For bonding microfluidic devices, it is used as a technique to change the surface properties of the polymer in order to decrease the temperature for subsequent thermal bonding. Therefore, a mercury lamp with the special emitting wavelength of 185 nm in an air-filled chamber generates ozone. The light is absorbed by oxygen and ozone is produced. The lamp has a second emitting wavelength, typically at 254 nm, which is simultaneously absorbed by the ozone. Within the closed chamber, a continuous generation and destruction of the ozone takes place, whereby a consistent concentration of atomic oxygen is developed, like it is shown in Equation 2.2.

[29]
Due to the high energy of the emitting UV radiation, the chemical bonds on the surface break. This opened binding sites want to reach a chemical stable state as fast as possible. Oxygen and ozone are reactants to bind on the surface of the polymer and new chemical compounds arise. [19, 28]

$$\begin{aligned} O_2 + h\nu(185nm) &\rightarrow 2\ O^* \\ O_2 + O^* &\rightarrow O_3 \\ O_3 + h\nu(254nm) &\rightarrow O_2 + O^* \end{aligned} \tag{2.2}$$

In the chamber, ozone acts as a strong oxidizing agent. It oxidizes the hydrocarbons on the surface of the polymers, which leads to a higher surface energy. Callen *et al.* [30] showed that the surface of polystyrene oxidizes due to UV/ozone treatment consisting of three different groups, C-O, C=O and O-C=O. The higher surface energy results in increased hydrophilicity and improved wettability. This fact allows bonding at lower temperatures and leads to higher bond strengths. However, this condition is unstable. Van Midwoud *et al.* [27] supervised the hydrophilicity after UV/ozone treatment of different polymers over 4 weeks. The first contact angle measurement was carried out 2 hours after the treatment. For the most treatment times the contact angle increased between 2 hours and 1 week after treatment. However, contact angles were not measured immediately after UV/ozone treatment, which could be an interesting period of time, too. Lin *et al.* [31] investigated the long-term behavior of the modified polymer surface for up to 16 weeks. They determined that the duration of the UV/ozone exposure and the storage conditions play an important role. The hydrophobic recovery can be inhibited by storing the substrates in vacuum or dehumidified conditions.
Berdichevsky *et al.* [32] investigated the penetration depth of PDMS by UV/ozone. They came to the conclusion, that the oxidized layer is about 10 µm, no matter if the duration of exposure is 30 or 230 minutes. In addition, the group measured the contact angles of PDMS after 30 minutes UV/ozone exposure and oxygen plasma treatment of one minute. They determined a slower hydrophobic recovery of the UV/ozone treated substrates compared to the oxygen plasma treated.

Therefore, measurements and thermal bonding have to be done timely after the

UV/ozone exposure. Advantages of this surface pretreatment by UV/ozone are the low costs and high throughput. Apart from this, the extra feature of cleaning the surface may also be an advantage, considering the preparation of the polymeric surface prior to exposure. The experimental setup can be arranged by commercial devices, such as those used for cleaning. [19, 28, 30]

2.4.1.2 Ultrasonic Welding

A common method of direct bonding is using ultrasonic energy to heat up the interface between the two polymer substrates. By heating, the interface is softened and the materials merged. It is possible to weld the surfaces locally only on specific regions, as well as globally.
Another advantage of this method is the relatively short duration of the bonding process. Its efficiency depends on the material, applied force used for even contact of the surfaces, welding frequency, welding amplitude, as well as welding time. In general, ultrasonic welding is suitable for bonding amorphous and semi-crystalline thermoplastic polymers. One problem that arises using ultrasonic welding for sealing the microchannels is the requirement of energy directors. Flat surfaces are not suitable for welding. Energy directors are the melting material and possible structures around them guide the melt flow in desired directions. This requirement complicates the design and fabrication of the microfluidic devices in terms of space and additional structures on the substrate. [4, 33]
Kistrup *et al.* [34] presented two different possibilities for energy directors, butt joint with energy director and tongue-and-groove joint as shown in Figure 2.10.
The first method is the most commonly used, because it is easier to implement. One disadvantage of this kind of director is the added height after it has been melted. If there is too much energy applied, the melted directors may flow into the channels. However, if there is insufficient energy applied on the directors, a small gap remains. These disadvantages are bypassed by using grooves like the tongue-and-groove joint, under consideration that both, the basis and the lid of the microfluidic device, must be adapted in terms of design. Furthermore, the angle of the energy director is depends on the thermoplastic polymer, which is 90° for amorphous polymers and 60° for semi-crystalline polymers. [34, 35]
Luo *et al.* [33] presented two novel methods for ultrasonic bonding, where no energy directors are needed. Due to preparation of the bonding interface by thermal and

solvent assistance prior to bonding, they found a way to bond without the need of energy directors. One method is based on the combination of solvent assisted bonding, using isopropanol as solvent, and ultrasonic welding. The second method is based on the combination of thermal assisted bonding and ultrasonic welding, where the substrates are preheated and welded by ultrasonic afterwards. [33]

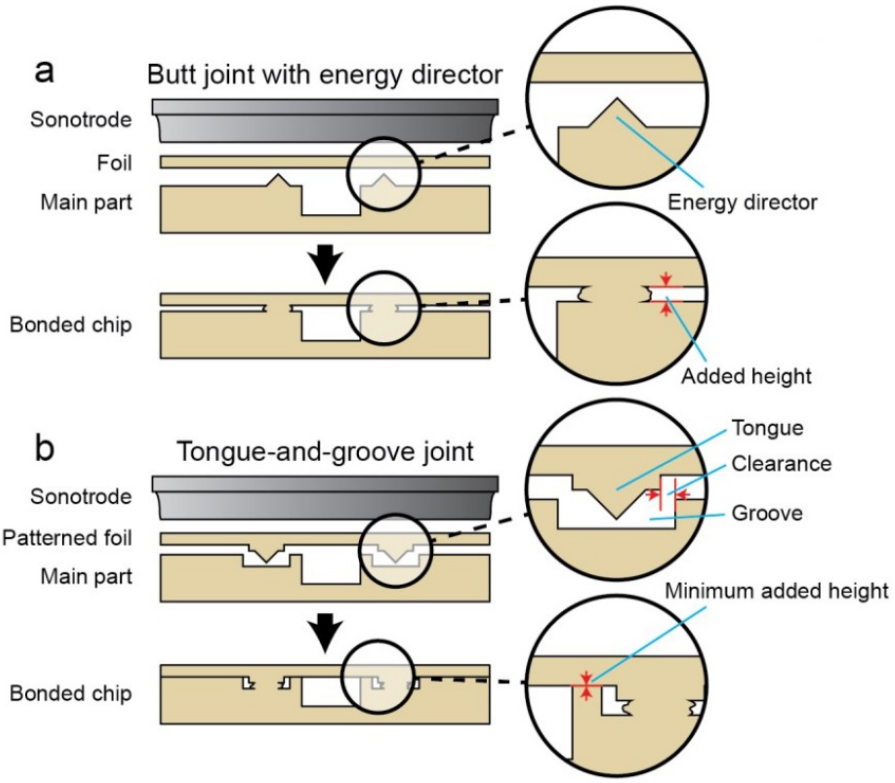

Figure 2.10: Two different energy directors for ultrasonic welding. (a) Butt joint with energy director, on the right in closer view with added height after bonding. (b) Tongue-and-groove joint where the material is captured in the groove after bonding. Figure taken from [34].

2.4.1.3 Laser Welding

Another direct bonding method is laser welding, which can be used very precisely. The most important requirements for applying laser welding are the different absorption coefficients of the base and the lid of the thermoplastic polymer device at the laser wavelength. For the precise heat induction at the bonding interface of the substrates, the layer near the laser source has to be transparent in order to reduce

the energy of the laser beam as little as possible. The base of the device has to be the absorbing layer to induce the heat precisely on the interface. The even contact of the two layers during welding is achieved by a clamping pressure. The laser sources usually have wavelengths in the near infrared region, i.e., between 800 nm and 1100 nm, and a power between 30 W and 400 W. One differentiates between contour welding and mask welding. During contour welding, the laser beam is driven by a XY mechanism along the regions of the desired bonding area. Contrarily, mask welding puts an absorbing or a reflective mask between the broad laser beam and the transparent layer of the microfluidic device. This mask covers the regions which should not be bonded. The quality of the bond depends on the beam and the mask quality. The advantage of contour welding in contrast to mask welding is the easily changeable path of the laser beam by reprogramming it. The disadvantage for contour welding is the speed. Due to the precise move of the laser along the contours, the process needs more time compared to mask welding. For mask welding, the mask, including difficult microstructures, has to be produced before the laser can be used, which reduces the flexibility compared to contour welding. [4]

2.4.1.4 Mechanical Joining

For mechanical joining, it is possible to join the polymer plates by ordinary screws or clamps. Another option is hot or cold caulking, where polymeric pins are pressed into prefabricated holes of the two substrates. The challenge of this method is to ensure tightness of the finished devices. A gasket around the channels might be required to guarantee a tight seal.

2.4.2 Intermediate Bonding Technologies

2.4.2.1 Adhesive Bonding

A very common method to seal microfluidic channels is by using adhesives. Liquid adhesives, which harden by mixing with a catalyzing agent, evaporation of solvent, or UV exposure are most commonly used. UV-curing adhesives are popular due to their physical and optical properties, solvent-compatibility and their ability to cure at low temperatures by UV. They are manufactured from synthetic resins con-

taining photoinitiators to raise the resin crosslinking when exposed to light of a specific wavelength. The challenges of adhesive bonding are applying the adhesive on the targeted areas, and with the same thickness over the whole area, and avoiding clogging of the channels by the adhesive. There are many approaches described in literature how to avoid channel clogging when applying adhesives for bonding substrates. Dang *et al.* [36] used a contact printing process, by applying the adhesive on a steel plate and spreading it with a blade. They dipped a silicon rubber pad into the adhesive and applied it onto the microchannel-containing polymer substrate. The thickness of the adhesive on the pad was smaller than the depth of the channels and so they remained free from adhesive. Riegger *et al.* [17] presented a technique for applying the adhesive via rolls and they designed capture channels. The best bonding conditions depend on the distance between the definition roll and the transfer roll, the viscosity of the adhesive and the transport velocity. They used a custom-built laminator for this technique. Another method for intermediate bonding is the application of adhesive sticky tape or lamination films. The easy process of sealing the channels with tape or film is attractive for fabricating microfluidic devices, because commercial laminators can be used. [4, 17, 18]
Regardless of the challenges associated with adhesive bonding, it has to be considered that intermediate bonding procedures go hand in hand with an inhomogeneity of the surface of the channel walls, because they consist of the polymer and the adhesive layer. This fact could be a disadvantage for using adhesives for bonding polymer microfluidic devices for medical applications. [33]

2.5 Quantification of Bond Strength

Bond strength is a characteristic of the bonded microfluidic device and shows how well the bonded parts hold together. This parameter can be used to identify differences in quality of the bonding interface with respect to the force needed to pull the parts apart. However, no statement can be made about the channel geometry; for example, if the channels are clogged or leaky. These characteristics have to be verified differently. In general, there is no test which is superior to all others, instead compromises must be made. The test should be selected depending on the requirements for every unique application. [37]
Literature provides different methods to determine the bond strength after the bond-

ing process have taken place. [23, 37, 38, 39]
The most common methods are the tensile test, shear test, and peel test, which are subsequently described.

2.5.1 Tensile Test

This test is relatively difficult to implement, because of the thin polymer material and the difficulty to mount the material on the tensile testing machine. For the fixation to the holder, epoxy is often used, but the challenge lies in not affecting the existing bonding interface while attaching the fixation. Nevertheless, the test fails mostly because the fixation ruptures and therefore no measurements are possible. Apart from this, a tensile testing machine is necessary which is associated with high costs. [23, 40]

2.5.2 Shear Test

The shear test is easier to implement than the tensile test. To measure the shear bond strength, it is necessary to prepare the substrates for the testing machine prior to bonding. The shear test cannot be performed for standard bonded devices with their desired functionality, because there is no option to attach the device to the machine. A possible solution could be to bond a small area of the material whereby jaws can fix the non-bonded parts. The load at failure can be determined and divided by the bonded area, the ultimate shear strength can be calculated. [23]

2.5.3 Peel Test

This test measures the force required for delamination. There are three different modes to realize the peel test: 90° peel off test, 180° peel off test, and the t-peel test. For the t-peel test, the substrates are delaminated in opposite direction, while the other modes show the delamination angles for peeling one of the parts. This method for testing the bond strength can be considered if at least one of the bonded substrates is flexible, e.g., a foil. For the t-peel test, both of the materials have to be flexible. [20, 23, 41]

2.5.4 Three-Point Bending Test

Apart from the methods mentioned above, there are three more to describe. Bhattacharyya *et al.* [28] verified the bond strength by performing a three-point bending test in a dynamic mechanical analyzer. In this case, two polymer parts with different sizes were thermally bonded, in which the smaller part was bonded in the middle of the larger one. The load-displacement curve shows the highest stress the bonded parts were able to withstand and characterizes the bonding strength. As for the shear test, it is necessary to prepare the substrates prior to bonding to perform this test. The bending test can also be carried out using four bending points. [28, 37]

2.5.5 Burst Pressure Test

Another method for testing the bond strength is the burst pressure test. Within this test, it is also necessary to prepare special bonded devices to execute the test. Keller *et al.* [38] realized the experimental setup by bonding a circular polymeric sheet on another bigger plate containing an access for compressed air. By increasing the pressure of the compressed air, the delaminating pressure can be measured or the bonded parts may withstand the maximum pressure of the compressed air line. In another study, a pressurized chamber was fabricated and a polymer plate was bonded on it. After pressurizing the chamber, delamination was detected due to formation of bubbles in a water bath. [25, 38]

2.5.6 Wedge Test

The last method to verify the bond strength is the wedge test, or crack-opening method, which belongs to the family of beam tests, like the three-point bending test. In first order, the equation was developed to calculate the bond strength between two silicon substrates. It is a commonly used method to characterize the interface of wafer bonding. The principle is based on inserting a blade of known thickness between the bonded substrates, whereby the occurring crack propagation length L is measured. The measurement can be done with an optical microscope or with a camera. The bond strength γ is calculated using the Maszara model [39], given by,

$$\gamma = \frac{3 \cdot t_b^2 \cdot E_1 \cdot t_{s1}^3 \cdot E_2 \cdot t_{s2}^3}{16 \cdot L^4 \cdot (E_1 \cdot t_{s1}^3 + E_2 \cdot t_{s2}^3)}, \tag{2.3}$$

where E is the Young's modulus, t_s is the thickness of the substrate, and t_b is the thickness of the blade. If the material of the bonded substrates is the same and have the same thickness, γ can be calculated by [19, 42]:

$$\gamma = \frac{3 \cdot E \cdot t_b^2 \cdot t_s^3}{32 \cdot L^4}. \tag{2.4}$$

Chapter 3

Techniques and Methods

In the subsequent chapter, the description of the experiments and used materials is presented. It gives answers on questions about the design of the experiment, the applied techniques to characterize the surface and the quality of the bonding interface. Furthermore, the chapter includes a description of the preparations, as well as the experimental setup for the measurements.

3.1 Kilobaser

The practical example for testing the UV/ozone surface modification prior to thermal bonding is a thermoplastic microfluidic chip developed for the Kilobaser. The Kilobaser is a development project by the company Briefcase Biotec GmbH in Graz, Austria, and is a device for synthesis of deoxyribonucleic acid (DNA). The chip is shown in Figure 3.1.

3.1.1 Design and Materials

The chip has the size of a standard microscope slide of 75 mm x 25 mm as can be seen in Figure 3.2. It consists of a base plate and a membrane plate. The base plate includes the channels with a height of 0.1 mm and a width of 0.2 mm. There are two small pins injection-molded on the side of the channels, which fit in the injection

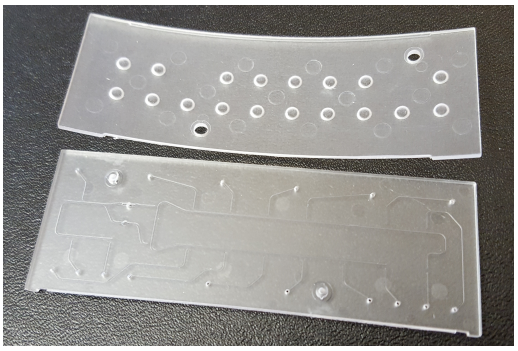

(a) The two parts of microfluidic chip. Above the two-component injection molded chip can be seen. Below the base plate with the microchannels is presented.

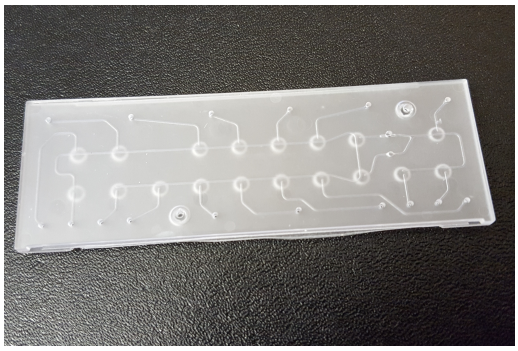

(b) The whole microfluidic chip.

Figure 3.1: The microfluidic chip of the Kilobaser. (a) The two parts of the chip, above the membrane plate, below the base plate. (b) The whole microfluidic chip.

molded holes of the membrane plate. The pins serve to support an even bonding process and they guarantee the perfect match of base and lid.

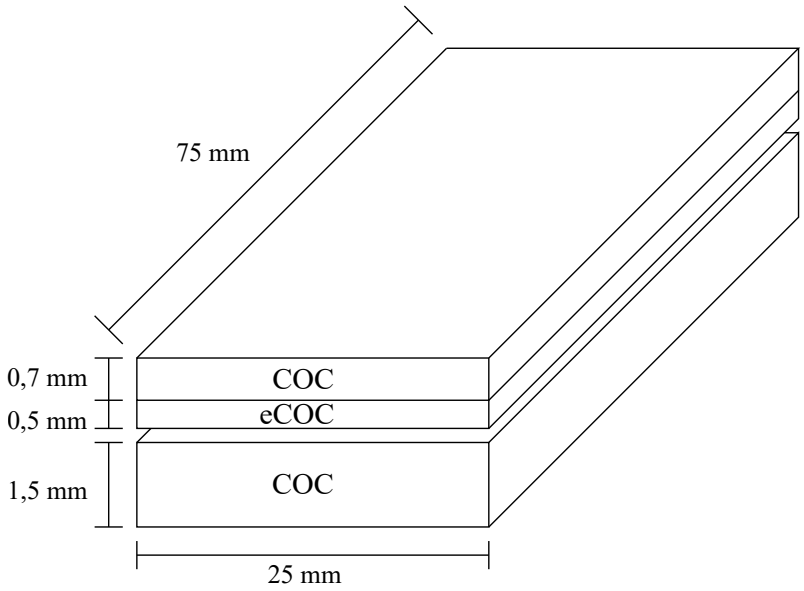

Figure 3.2: Heights and size of base and membrane plate (not to scale).

The base of the microfluidic device is injection-molded from COC (Topas® 8007S-04, Topas Advanced Polymers, Germany). The membrane plate is a two-component injection-molded part. The non-bonded side is made of the same material as the base plate. The side of the membrane plate which is bonded on the base and seals

the channels is the second component, made of eCOC (Topas® Elastomer E-140, Topas Advanced Polymers, Germany). The eCOC is a relatively new polymer and is barely described in microfluidic literature. Table 3.1 lists some material parameters, taken from [43, 44].

Table 3.1: Material parameters for COC and eCOC, taken from data sheets [43, 44].

	T_g [°C]	T_m [°C]	E [MPa]
Topas® 8007S-04	78	-	2600
Topas® Elastomer E-140	-	84	50

The membrane plate has small holes injection molded in the COC component. The eCOC component is injection molded over the holes. Therefore, after bonding the two parts of the chip together, valves arise, due to the elastic component. These valves can open at a specific time, using small pressures, when a reagent has to be added to the synthetization of primer DNA.

3.2 UV/Ozone Surface Treatment

As a focus of this thesis, the base and the membrane plate are bonded by thermo-compression bonding and surface modification by UV radiation prior to bonding. The decision for the bonding technique was made according to the exclusion criterion: the design of the base plate does not have space for energy directors for ultrasonic welding. Both parts of the chip are transparent, so laser welding was not an option either. The space between the channels is very small, therefore the risk is high to clog the channels by the adhesive in case of adhesive bonding. Furthermore, there is no place for designing capture channels. The risk of leaky channels was estimated to be too high for techniques of mechanical joining, beside of this, there is no space for screws or pins for hot or cold caulking. Thus, thermal bonding was the most suitable way to bond the polymer device, because of its easy implementation and the lower costs compared to other technologies. The surface pretreatment via UV/ozone was realized by an U-shaped, ozone-generating, low-pressure mercury lamp (Heraeus Holding GmbH, Germany) with emitting wavelengths of 185 nm and 254 nm. It was attached inside on the top of an absorbing black box and connected

to a timer for a precise timing of UV exposure. The surfaces of the microfluidic base plate and the membrane plate, which had to be bonded together, were exposed by the UV radiation between 0 minutes and 20 minutes in an interval of 5 minutes for contact angle measurements, whereas a shorter interval was used for Attenuated Total Reflection Infrared Spectroscopy (ATR-IR) Spectroscopy. The limits were set on the basis of literature research and the time aspect of the bonding process. Due to the fact that it is only possible to place two bases and two lids in the box under the light source at the same time, the exposure time should not be too long. To determine the duration of UV exposure with the best outcome, the surface of the exposed polymer plates was characterized with techniques explained in Section 3.3.

3.3 Surface Characterization

To determine the results of the UV/ozone treatment, the surface of the polymeric plates were examined. The surface was characterized using the following techniques:

- Contact Angle Measurement
- Attenuated Total Reflection Infrared Spectroscopy.

As mentioned in Section 2.4.1.1, the effect of UV/ozone exposure does not last a long time and the measurements have to be done timely after the exposure.

3.3.1 Contact Angle Measurement

The surface of an untreated substrate fabricated by COC is hydrophobic. To enhance adhesion properties, it is necessary to improve wettability. To define the wettability of a substrate, the contact angle can be measured. Therefore a liquid, mostly deionized (DI) water, is dropped on the polymeric plate. The plate has to lie flat and horizontal, and the angle formed by the intersection of liquid-vapor and liquid-solid interface is measured by applying a tangent line. In general, one speaks of superhydrophobic surfaces for contact angles greater than 90° . Contact angles of hydrophobic surfaces are at about 90° , whereas the contact angles of hydrophilic surfaces are less than 90°, as can be seen in Figure 3.3. Complete wetting occurs at a contact angle of nearly 0° , like a drop of DI water on a clean glass slide.

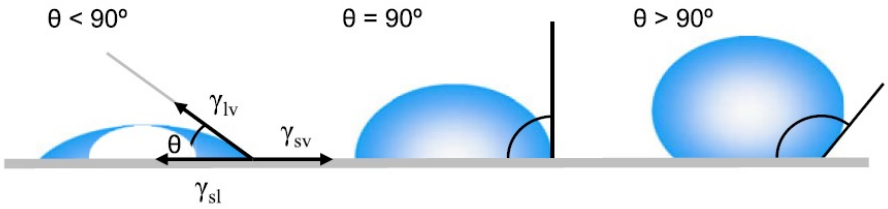

Figure 3.3: Definition of contact angles, taken from [45].

Surface tension is responsible for the typical shape of a drop. Every molecule in a pure liquid is pulled equally in every direction by the neighboring molecules resulting in a force of zero. The molecules at the liquid-vapor and at the liquid-solid interface do not have neighboring molecules in all directions, they are pulled inwards instead. The result is a contracting surface of the liquid and the surface tension, which gives the drop its shape. Gravity has an impact on shape of the drop and the contact angle is therefore affected by surface tension and gravity. Thomas Young described in 1805 that the surface tension of a liquid drop on an ideal surface is a mechanical equilibrium of three interfacial tensions [45], given by,

$$\gamma_{lv} \cos \Theta_Y = \gamma_{sv} - \gamma_{sl}, \tag{3.1}$$

where γ_{lv}, γ_{sv}, and γ_{sl} are the tensions of the interfaces, liquid-vapor, solid-vapor, solid-liquid, and Θ_Y is the contact angle. Equation 3.1 is known as the Young´s equation.

The contact angles were determined by using the professional contact angle measurment device OCA 15EC (DataPhysics Instruments GmbH, Germany) by depositing a 5 µl drop of DI water, on the plates, as shown in Figure 3.4.

The angles were calculated by the SCA 20 software provided by the manufacturer of the instrument. The measurements were done for the base plate and the membrane plate seperately. The drop was dispensed on the side of exposure. So for the membrane plate of the device, the examined material was eCOC and for the base plate it was COC. To determine the contact angle of the untreated material, the measurement was taken without prior UV/ozone exposure for both parts. The measurements were performed after 5, 10, and 20 minutes of UV/ozone exposure. 20 minutes were considered as an extreme value to check whether a longer exposure

Figure 3.4: 5 µl drop of DI water out of syringe of the contact angle measurement device.

time show reduced contact angles compared to shorter exposure times. The drop was dispensed on three different locations on the surface and nine measurements for every exposure time were performed. The measurement of the contact angle of the membrane plate was only possible in the center of the chip, because the eCOC component was not flat-bottomed but bulged. It was fixed with sticky tape on the table of the contact angle measurement device. The reason for the curvature of the membrane plate is the elastomeric component. Therefore, the base plate made of COC is flat-bottomed and the measurements were easier to perform.

3.3.2 ATR-IR Spectroscopy

Another possible measurement technique to investigate surface properties and material characteristics is spectroscopy. Attenuated Total Reflection Infrared Spectroscopy is a very common analytical technique, mainly used for identification. The absorption of the infrared radiation results in excitation vibration of the bonds. The resulting vibrations can be seen in the spectrum. Each chemical bond has its own infrared characteristic and can therefore be verified due to the peaks in the spectrum

at specific wavenumbers. The wavenumber indicates how often a bond oscillates per unit length. For the examination of the surface of the polymeric parts, ATR-IR Spectroscopy was used to determine the spectra of the modified surfaces. The special case of a ATR-IR Spectroscopy is that a crystal in which multiple reflections are possible. So the crystal has a high refractive index. If the sample is in contact with the crystal, the detector collects the changes of the infrared beam when it exits the crystal. The penetration depth of the beam into the surface of the polymer is about 0.5 µm to 5 µm.

The measurements were done with an ATR-IR Spectroscope, Bruker Tensor 27 (Bruker Corporation, USA). The software OPUS used to determine the spectra was provided by the manufacturer of the spectroscope. The ATR-IR Spectra were measured without surface modification after 1, 2, 5, 10, 15 and 20 minutes of UV/ozone exposure with 4 samples for each duration. To check whether there was a homogeneous irradiation of the plates under the lamp, for each exposure time one sample was measured on different positions. As crystal material a germanium crystal was used. Before the measurements could be done, background measurements had to be performed to compensate environmental influences.

3.4 Design of Experiment

This subsection contains the description of the experiments performed to determine the most reliable bonding parameters. Principally, the surface of the base and the membrane plate were exposed to UV radiation and bonded afterwards in a commercially available hot press. Then the characterization of the bonded layer was carried out. The heat press used was a pneumatic press (DSMC, Model DS-1B0810, China), where time and temperature can be set manually. The first step considering the design of experiment was to define several bonding parameters, and to establish the fix given and the variable ones. The parameters which had to be considered are summed up in Table 3.2.

Because of the cleaning effect of a UV/ozone treatment, a seperate cleaning step of the base and membrane plate surfaces were omitted. Based on the results of the surface characterization, the exposure time was fixed at 10 minutes for both the base plate and the membrane plate. The distance between the substrates and

Table 3.2: Fixed and variable set bonding parameters.

	fixed	**variable**	**steps/measures**
surface cleaning	x		none
exposure time	x		10 minutes
substrate lamp distance	x		7 cm under lamp
temperature during exposure	x		room temperature
atmosphere	x		air
time between UV exposure and bonding	x		immediately
bonding temperature		x	60 ℃ to 80 ℃ / interval of 5 ℃
bonding pressure	x		2 bar
bonding time		x	5 and 10 minutes
holding pressure	x		holding pressure = 0 Pa
holding time	x		holding time = 0 min

the lamp was fixed to 7 cm. The laboratory circumstances, room temperature and atmospheric air, were accepted during exposure. As mentioned above, the surface modification due to UV exposure does not last a long time, so the substrates were bonded immediately after the exposure. The bonding temperature was varied between 60 ℃ and 80 ℃ in increments of 5 ℃ to stay under the T_g and T_m of the substrates. This reduced the risk of clogging or deforming the channels. The bonding pressure was set to 2 bar of compressed air and due to the fixed radius of the pneumatic cylinder, the resulting force, the cylinder can apply can be determined as in Equation 3.3.

$$\begin{aligned} p_{ca} &= 2\,\mathrm{bar} = 200000\,\mathrm{N/m^2} \\ r_{cyl} &= 0.0315\,\mathrm{m} \end{aligned} \tag{3.2}$$

$$\begin{aligned} A_{cyl} &= r_{cyl}^2 \cdot \pi = 0.0315\,\mathrm{m}^2 \cdot \pi = 0.00312\,\mathrm{m}^2 \\ F_{cyl} &= p_{ca} \cdot A_{cyl} = 200000\,\mathrm{N/m}^2 \cdot 0.00312\,\mathrm{m}^2 = 624\,\mathrm{N} \end{aligned} \tag{3.3}$$

The resulting pressure on the microfluidic chip was calculated according to Equation 3.4.

$$\begin{aligned} A_{chip} &= 0.025\,\mathrm{m} \cdot 0.075\,\mathrm{m} = 1.88 \cdot 10^{-3}\,\mathrm{m}^2 \\ p_{chip} &= \frac{F}{A} = \frac{624\,\mathrm{N}}{1.88 \cdot 10^{-3}\,\mathrm{m}^2} = 331915\,\mathrm{N/m}^2 = \ 332\,\mathrm{kPa} \end{aligned} \tag{3.4}$$

This pressure was high enough to ensure an even contact between the mating surfaces, so a higher pressure of compressed air was not considered to be necessary. For lower pressures like 1 bar, the application was too risky in case of the unreliable function of the pneumatic cylinder for this pressure. Because of these reasons, the pressure was constantly set to 2 bar.

The bonding time was varied between 5 and 10 minutes. The holding pressure and holding time was 0 minutes, because the heat press is not able to hold the pressure without temperature after the bonding time is over.

3.4.1 Applied Bond Strength Verification Methods

After the process parameters were set, the decision about the bonding strength verification method had to be made. In Section 2.5, the most common methods to verify the bond strength found in literature are summarized. Because there was no machine available to perform tensile, shear or peel tests, these tests could not be performed on the bonded substrates. The device needed to perform a three point bending test was not available, too. Therefore, the burst pressure test and the wedge test were performed.

3.4.1.1 Burst Pressure Test

To perform the burst pressure test, the substrates had to be specially prepared prior to bonding. A hole with a diameter of 2 mm was drilled in the middle of the base plates, an area where no channel geometries were injection molded. The shape of

the membrane plate was modified to a small circular plate with a diameter of 10 mm, which was punched out of the two component substrate, as shown in Figure 3.5 (a). After the UV/ozone exposure, the membrane plate was bonded in the middle of the hole on the back side of the base plate. The back side was chosen, because there are no channels and the bonded area is continuous and not interrupted. There should be no different behavior because the material of the base is the same. To connect the hole in the base plate with compressed air a special clamping tool was designed. As shown in Figure 3.5 (b), a hole with a larger diameter than that of the punched membrane plate was drilled in the upper aluminium plate. Four holes were drilled at the edges to screw the two plates together. The connector for the compressed air line was fixed on the back side of the clamping tool, as can be seen in Figure 3.5 (c).

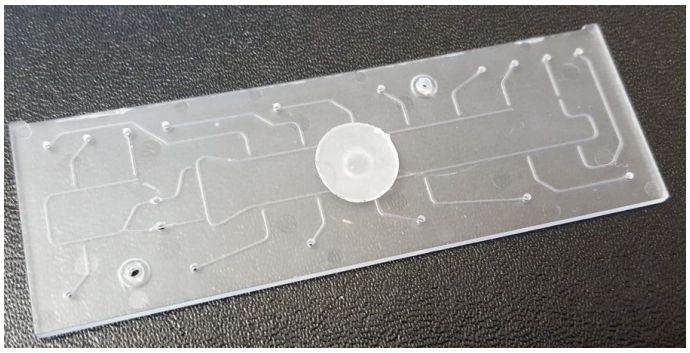

(a) Modified substrate

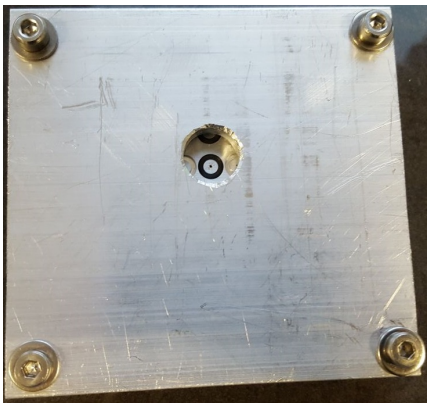

(b) Front of the Clamping tool

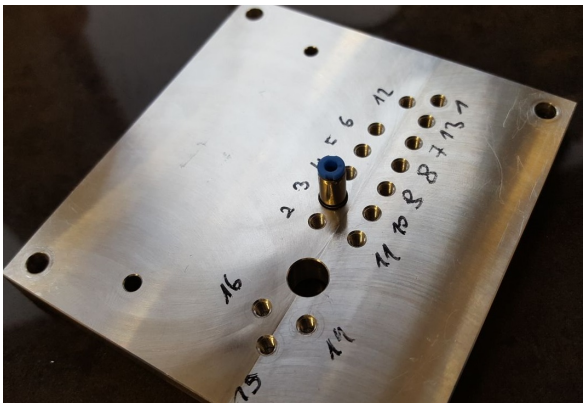

(c) Back of the Clamping tool

Figure 3.5: Specially prepared substrates and clamping tool. (a) Prepared base plate with the hole and the punched membrane plate. (b) Front side of the specially designed clamping tool. (c) Back side of the clamping tool with the connection to compressed air.

A groove was milled in the lower plate to fix an o-ring with the same diameter as the hole of the base plate. The bonded substrates were positioned between the two aluminium plates and fixed by tightening the srews. The hole of the base was positioned on the o-ring of the aluminium plate. The compressed air was forced into the modified substrate and the air pressure increased until the bonding was leaking. The leakage was determined acoustically by the sound of a whistle.

3.4.1.2 Wedge Test

The wedge test was also used to determine the bond strength. In this case, the microfluidic device did not have to be modified or specially pretreated, but could be bonded in the original, functional way. The chosen blade was a commercially available cutter knife, with a thickness of 0.38 mm by OLFA® (OLFA Corporation, Japan). After the bonding process under varied parameters, the blade was carefully inserted between the two layers, always until the width of the blade was fully inserted between the bonded substrates, as shown in Figure 3.6. The resulted crack length was optically measured by a microscope camera, Moticam 3.0 MP (Motic Deutschland GmbH, Germany), which was connected to a laptop by a USB interface. The software, Motic Images Plus 3.0, was provided by the company. After the camera was calibrated by using the included templates, the crack length could be measured by applying a straight line from the beginning of the blade to the bond-air interface.

To ensure an equal execution of the wedge test, the longest crack length was evaluated. To improve the contrast for measurement of the crack length, a black pad was placed under the transparent polymer substrates.

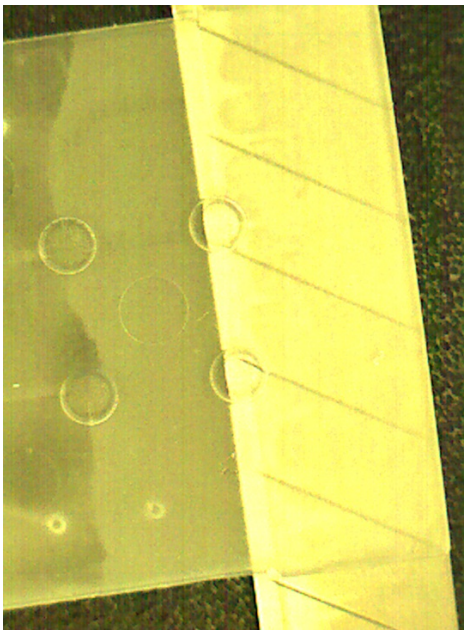

(a) Inserted blade with resulting crack length.

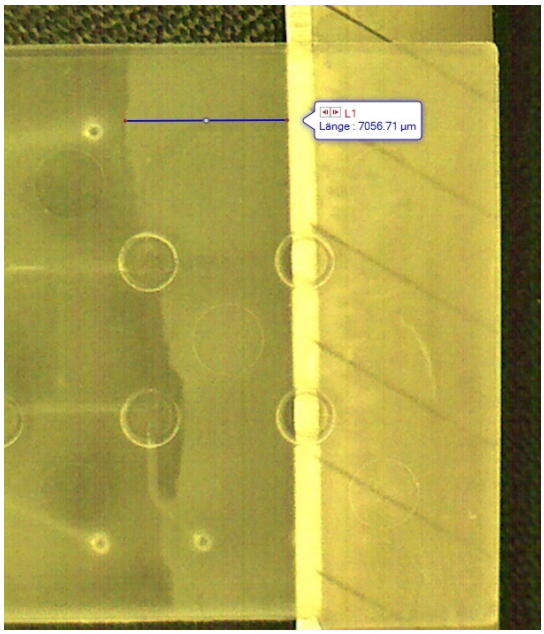

(b) Inserted blade with measured crack length.

Figure 3.6: Inserted blade between the bonded polymer parts. (a) Fully inserted blade and resulting crack length. (b) Measured the largest crack propagation from the tip of the blade.

Chapter 4

Results

The subsequent chapter summarizes the results of the surface characterization and the bonding experiments. For the calculation of the results, two types of software were used. RStudio was used to create statistical calculations. Diagrams and fitting calculations were done with MATLAB® (The MathWorks, Inc.). The codes for the calculations are presented in the Attachment section.

4.1 Surface Characterization

The decision to continue the bonding experiments with 10 minutes UV/ozone exposure time for the best bonding outcomes was made based on the results of the measurements for surface characterization, as presented in Section 4.1.1 and Section 4.1.2.

4.1.1 Contact Angle Measurement

The results of the contact angle measurement show definetly a decrease of the contact angle for higher exposure times. Figure 4.1 shows an example picture of the contact angle of the chip base without (a) and after 10 minutes (b) UV/ozone surface modification. In Figure 4.2, the mean values (N=9 for the base plate, N=3 for membrane plate) of the contact angle measurements for different exposure times are presented.

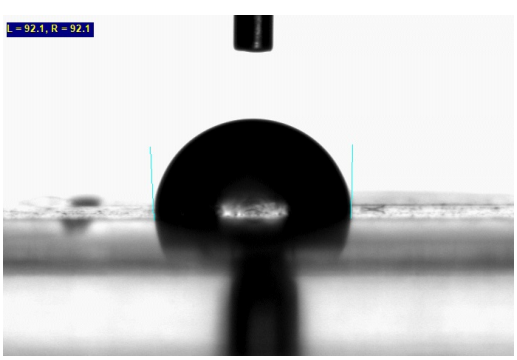

(a) Contact angle of chip base prior to UV/ozone exposure.

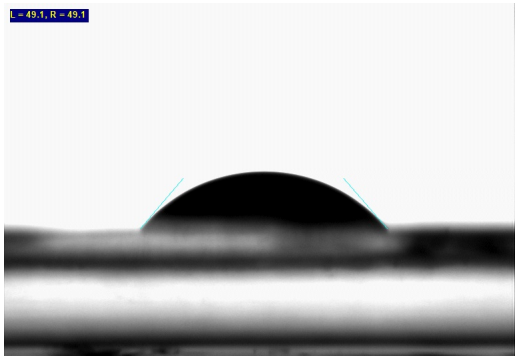

(b) Contact angle of chip base after 10 minutes UV/ozone exposure time.

Figure 4.1: Contact angle of chip base (a) Contact angle without prior UV/ozone exposure. (b) Contact angle after 10 minutes UV/ozone exposure time.

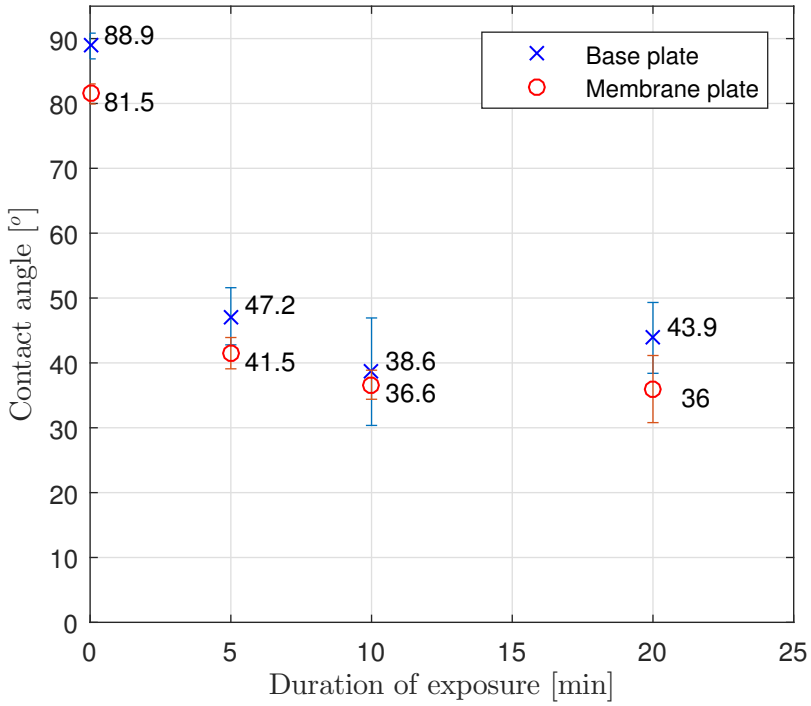

Figure 4.2: Results of the contact angle measurements, with bars representing the standard deviation of the results.

The contact angles of the membrane plate are always smaller than the contact angles of the base plate. This difference may be caused by the elastomeric part of the COC. For the first 5 minutes of UV/ozone exposure, the contact angles decrease to almost half of the contact angles of the untreated surface. For the next 5 minutes

of exposure, the contact angles continue to decrease but the negative slope is much smaller compared to the first 5 minutes. After 10 minutes of exposure, there is no further significant decrease of the contact angles detectable. The results show an increase of the surface wettability due to UV/ozone exposure and a saturation of surface wettability after 10 minutes.
Tsao *et al.* [19] measured contact angles of COC after different exposure times, too. Compared to their results, the contact angles presented in Figure 4.2 are some degrees smaller for each temperature. However, the standard deviation of the angles is much lower for the results presented by Tsao *et al.* [19]. They reported a contact angle without exposure at about 94.7° ± 1.0°, which is about 6° higher than the contact angle presented in this research. Similar results show the fact that after 10 minutes UV/ozone exposure no significant decrease of the contact angle is detectable.
Bhattacharyya *et al.* [28] measured contact angles of COP after different exposure times and the results are comparable to them of this research. They reported a decrease of the contact angles after 5 minutes from about 95° to about 52°.
No information was found in literature about the decrease of contact angles of eCOC.

4.1.2 ATR-IR Spectroscopy

4.1.2.1 Base Plate - COC

As shown in Figure 4.3, the ATR-IR spectra for different positions on one sample are very similar, which suggests a homogeneous distribution of the UV/ozone irradiation.

Roy *et al.* [26] described the dominant peaks in 2940 - 2860 cm^{-1} for the CH stretching mode and at about 1454 cm^{-1} for the CH bending mode, and found a good match between this peaks in literature. The transmission peak, at around 1744 cm^{-1}, is the presence of carbonyl and aldehyde groups. The peaks at the mentioned wavenumbers can be seen in Figure 4.4, where different spectra for different exposure times are presented. The spectra can be compared directly, where a decreasing transmission at around 1744 cm^{-1} is detecable for increasing exposure times, as shown in Figure 4.4 (b). This means that the number of carbonyl and aldehyde groups increases for longer UV/ozone exposure of the COC base plate. [26]

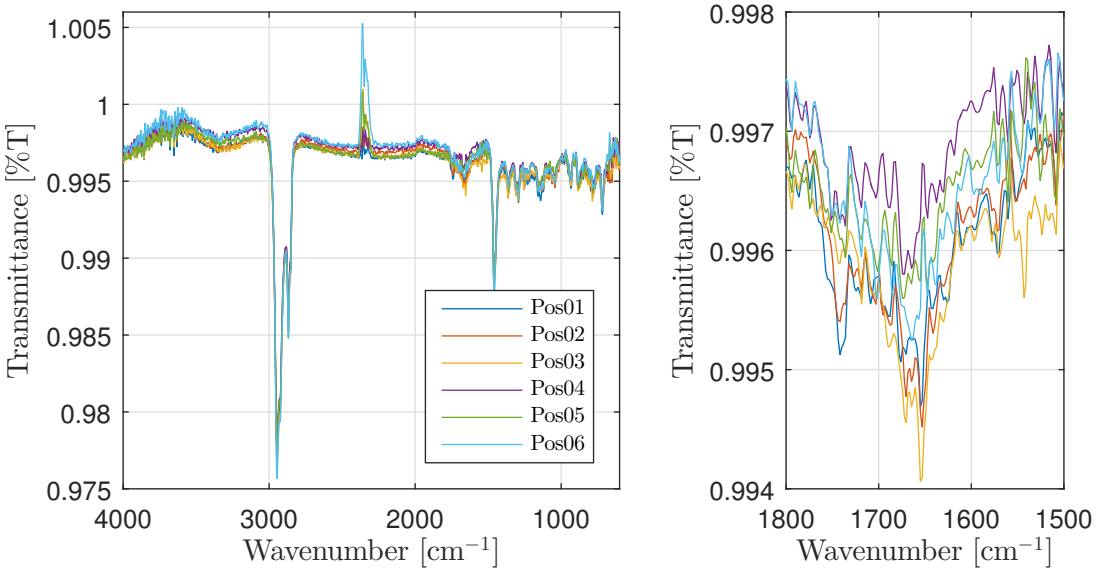

(a) IR-spectra of 2 minutes exposed base plate on different positions

(b) Detailed figure, with the same legend as in (a).

Figure 4.3: ATR-IR Spectra of 2 minutes exposed base plate on different positions. (a) Whole spectrum of 2 minutes exposed base plate on different positions. (b) Detailed figure of range of interest.

The peak at the wavenumber of 2340 cm^{-1} shows most of the measurements very different heights. This peak indicates the presence of CO_2 in the laboratory where the measurements were examined. The difference in transmission is indicated by different amounts of people working in the laboratory while the measurements were done. Because the expected occuring peaks were not near the wavenumber of CO_2, no correction of this peak was considered to be necessary.

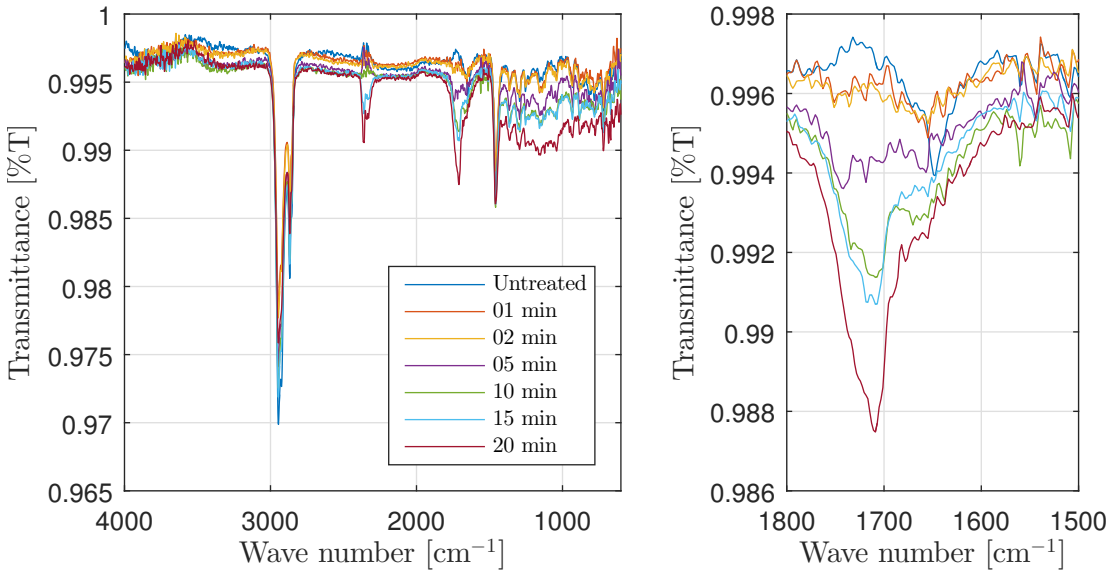

(a) IR-spectra of different exposure times of base plate

(b) Detailed figure, with the same legend as in (a).

Figure 4.4: ATR-IR-Spectra of different exposure times of base plate. (a) Whole spectrum of different exposure time of base plates. (b) Detailed figure of range of interest.

4.1.2.2 Membrane Plate - eCOC

The ATR-IR spectra of the membrane plates show less noise compared to the spectra of the base plate. The reason for this fact could be the roughness of the surface. The roughness of COC is higher compared to eCOC. Therefore, no plane contact to the crystal is possible and this let suggest that entrapped air might be the reason for the higher noise for the COC spectra.
One unexpected problem occured during the measurements. Due to the pressure applied on the plate for an even contact to the germanium crystal, the eCOC stuck on the crystal. For this reason, the ATR-IR spectra were measured only at three positions of one sample for each exposure time. In Figure 4.5, the problem is detectable as a big drift of the transmittance.

Due to the sticky eCOC, it is possible that there were polymeric residues on the germanium crystal, which means that the measured spectra were falsified and therefore do not show the right spectra of one polymer slide. In Figure 4.6, the spectra of different exposure times are summarized in one plot. Again, it is visible that

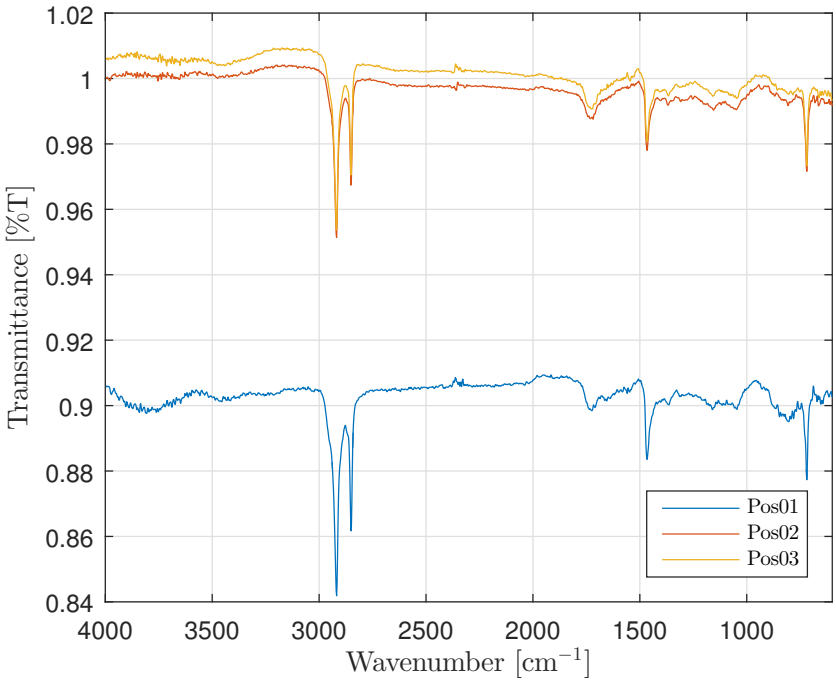

Figure 4.5: ATR-IR spectra of a membrane plate exposed to UV/ozone for 15 minutes at different positions.

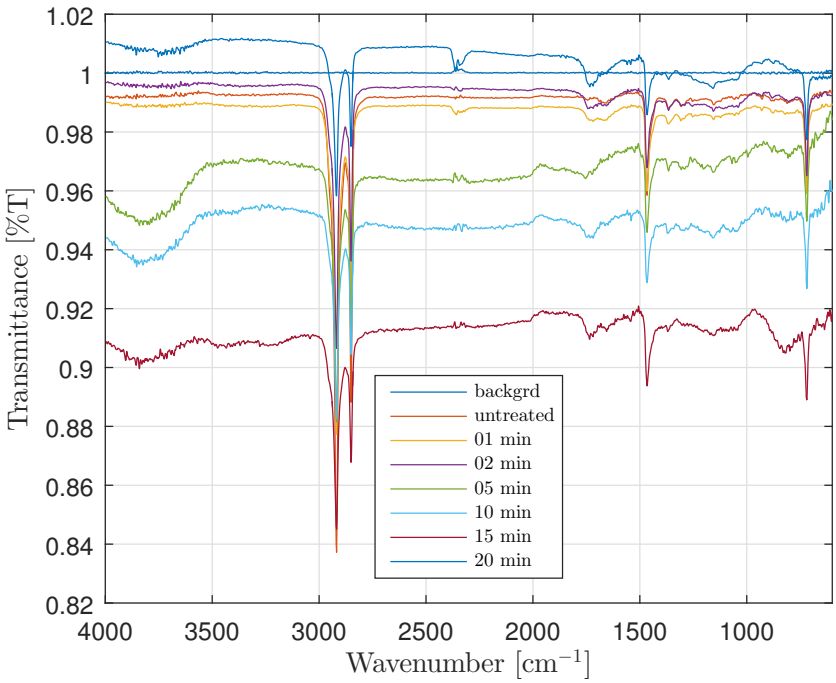

Figure 4.6: ATR-IR spectra of different exposure times of a membrane plate.

undesirable polymeric residues were included in the measurements.

4.2 Experiments - Thermocompression Bonding

After the investigation of changes of the surfaces due to UV/ozone exposure, the bonding process was investigated by varying the temperature and the pressure holding time of the hot press, as explained in Section 3.4.

4.2.1 Burst Pressure Test

For the results of burst pressure test, the compressed air pressure where the bonded parts leaked, was determined, as shown in Table 4.1, and the burst pressures were calculated afterwards. In Equation 4.3, a calculation example for the burst pressure is presented.

Table 4.1: Raw data of burst pressure test.

Bonding Temperature [^oC]	**Leak Pressure [bar]**
60	1
60	3
60	2
65	2.5
65	7
65	4.5
70	7
70	5
70	6
80	7
80	7
80	7

$$\begin{aligned} A_{hole} &= \pi \cdot r^2 = \pi \cdot (0.001 \text{ m})^2 = 3.14 \cdot 10^{-6} \text{ m}^2 \\ A_{bonded\ area} &= \pi \cdot r^2 - A_{hole} = \pi \cdot (0.005 \text{ m})^2 - 3.14 \cdot 10^{-6} \text{ m}^2 = 75.4 \cdot 10^{-6} \text{ m}^2 \\ p_{comp\ air} &= 700000 \text{ Pa} \end{aligned} \tag{4.1}$$

$$F = p_{comp\ air} \cdot A_{hole} = 700000 \frac{N}{\text{m}^2} \cdot 3.14 \cdot 10^{-6} \text{m}^2 = 2.2 \text{ N} \tag{4.2}$$

$$\sigma_{burst} = \frac{F}{A_{bonded\ area}} = \frac{2.2 \text{ N}}{75.4 \cdot 10^{-6} \text{m}^2} = 29178 \text{ Pa} \tag{4.3}$$

In general, this method to verify the bond strength was dicarded because of two reasons. The technique was not reproducable and it was inaccurate in case of hearing the leak by increasing the compressed air pressure. Because of this, three samples were taken for each temperature. Nevertheless, in Figure 4.7, where the calculated results are presented, a tendency of higher burst pressures for increasing temperatures can be seen.

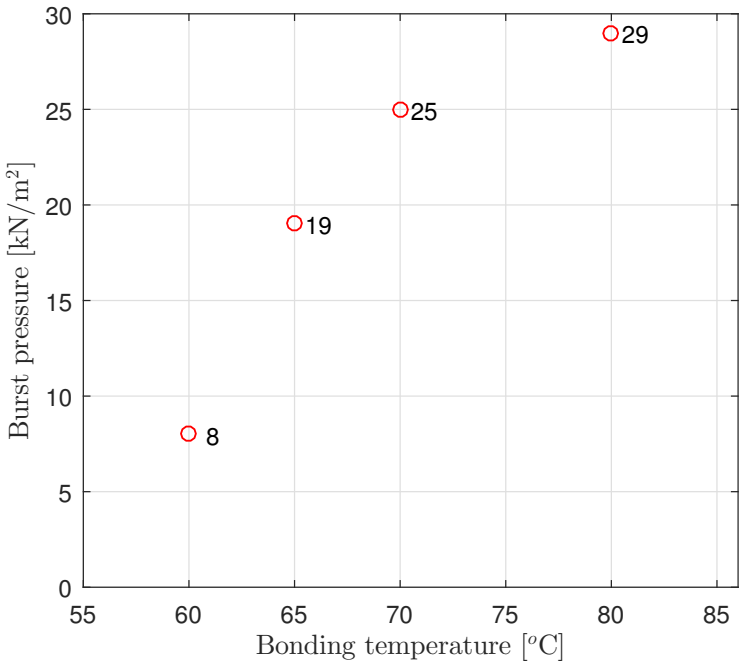

Figure 4.7: Results of burst pressure test (Median N=3, pressure holding time = 5 minutes).

4.2.2 Wedge Test

The raw data of the wedge test are listed in Table 4.2, where the red marked value is the chosen value for the calculation example presented in Equation 4.5. The equation presented in Section 2.5.6 shows the calculation of the bond strength. The Young's modulus for the membrane plate was the one for COC, and the thickness was taken from the COC component under the assumption that the elastomeric component has minor influence on the stiffness of the material.

$$\begin{aligned} \text{pressure holding time} &= 10 \text{ min} \\ \text{UV/ozone exposure time} &= 10 \text{ min} \\ T_{set} &= 65°\text{C} \\ t_b &= 380 \ \mu\text{m} \\ L_{measured} &= 7948.08 \ \mu\text{m} \end{aligned} \tag{4.4}$$

$$\begin{aligned} \gamma &= \frac{3 \cdot (0.38 \text{ mm})^2 \cdot 2600 \text{ MPa} \cdot (1.5 \text{ mm})^3 \cdot 2600 \text{ MPa} \cdot (0.7 \text{ mm})^3}{16 \cdot (7.95 \text{ mm})^4 \cdot (2600 \text{ MPa} \cdot (1.5 \text{ mm})^3 + 2600 \text{ MPa} \cdot (0.7 \text{ mm})^3)} \\ \gamma &= 5.492 \ \frac{\text{J}}{\text{m}^2} \end{aligned} \tag{4.5}$$

Table 4.2: Raw data of wedge test, where the red value represents the value of the calculation excample.

Bonding Temperature [°C]	**Crack Length [µm]**	**Bonding Temperature [°C]**	**Crack Length [µm]**
60	10344.61	65	8599.37
60	18227.49	65	8426.10
60	12924.44	65	8252.34
60	33979.56	65	7636.57
60	11723.46	65	7948.08
60	11836.87	65	7333.02
60	13078.15	65	7249.83
60	11217.71	65	9141.81
70	6740.29	75	4737.56
70	6247.90	75	4042.39
70	5681.52	75	6254.90
70	7056.71	75	4767.63
70	6442.52	75	5095.26
70	7916.31	75	5822.79
70	11563.09	75	5282.95
70	6325.01	75	4165.27
80	2716.82		
80	2080.48		
80	2137.94		
80	2588.16		
80	3782.09		
80	2751.08		
80	5323.33		
80	2430.55		

4.2.2.1 Effect of 0 and 10 minutes UV/Ozone exposure on bond strength

To determine the difference between bond strengths of prior UV/ozone treated and non-treated substrates, four samples were bonded for each temperature without

prior UV/ozone exposure. Figure 4.8 shows the difference of the medians of bond strengths for 0 and 10 minutes of exposure for different bonding temperatures. The pressure holding time was set to 5 minutes for both groups.

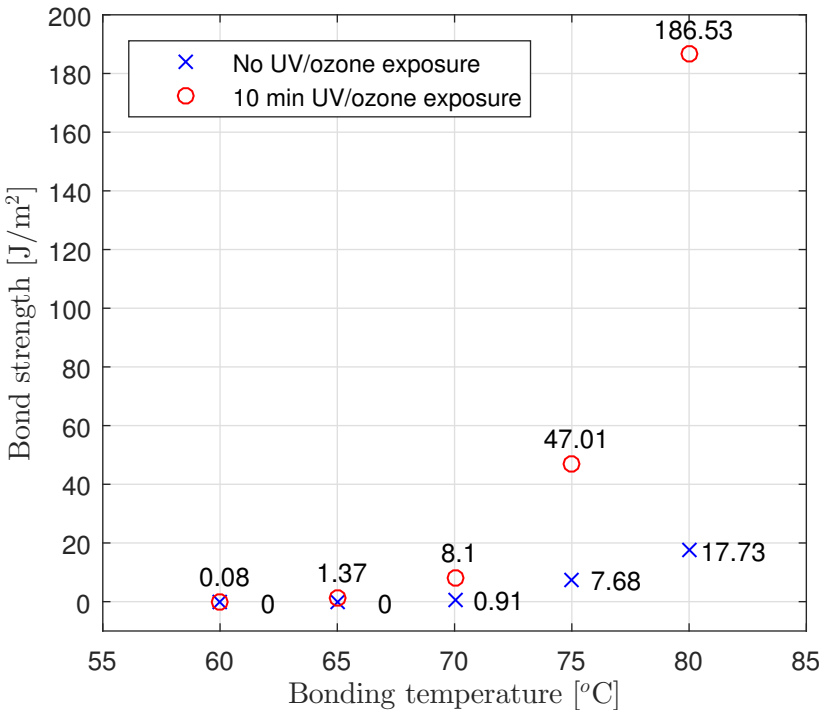

Figure 4.8: Comparison between 0 and 10 minutes of UV/ozone exposure.

To check whether the calculated values for bond strength are normally distributed, the Shapiro-Wilk-Test was performed using the programming language R. The Shapiro-Wilk-Test can be used for $3 \leq N \leq 5000$, where N is the number of samples. The number of samples was 4 for the non-exposed devices and 8 for 10 minutes exposure time. As a level of significance, the value 0.05 was chosen, i.e., $\alpha = 0.05$. The null hypothesis (H_0) assumes that the population is normally distributed.
The results of the Shapiro-Wilk-Test showed p-values greater than 0.05 which means that H_0 can be accepted and the data of bond strengths can be assumed to be normally distributed for bonding temperatures greater than 65 °C for non-exposed samples. The values for 60 °C and 65 °C bonding temperature were the same, because the crack length was considered as maximum, 7 cm. For these samples, it was not possible to measure any length because they fell apart immediately. These data are not normally distributed. Quite similar are the results for the 10 minutes exposed devices. The p-values for 60 °C and 65 °C are smaller than 0.05, so H_0 has to be

rejected and the data are not normally distributed. For temperatures greater 65 °C, H_0 can be accepted and it can be assumed that the data are normally distributed. Because of the normally distributed data, the unpaired t-test was performed using R to check whether there is a significant difference between the bond strengths of 0 minutes and 10 minutes of UV/ozone exposure. The results of the t-test showed that there is a significant difference ($p < 0.05$) of the bond strength between 0 and 10 minutes UV/ozone exposure prior to bonding for 70 °C, 75 °C and 80 °C.
In comparison to the results presented by Tsao *et al.* [19], they achieved much lower bond strengths compared to the results presented in Figure 4.8. The bonding procedure of the group is quite similar to the procedure presented in this thesis. They calculated bond strength using the wedge test method, and modified the surfaces of COP by UV/ozone prior to bonding in a hot press. Nevertheless, the group made one step additional prior to bonding. They rinsed the samples with 2-propanol and DI water, dried them and left the samples in a vacuum oven for two hours. This might be the reason for the lower bond strengths compared to the results presented in this thesis.

4.2.2.2 Effect of 5 and 10 minutes pressure holding time on bond strength

The median values (N=8 for 10 minutes pressure holding time, M=10 for 5 minutes pressure holding time) and the coefficient of variation (CV) of the samples are shown in Table 4.3 for 5 and 10 minutes pressure holding time for 60 °C to 80 °C in steps of 5 °C. CV gives an impression of the scattering of the values. It is calculated by standard deviation (σ) divided by the arithmetic mean (µ). It is a standardization of variance.

The medians of the bond strengths are higher for 10 minutes pressure holding time, except for bonding temperature set at 75 °C, as shown in Figure 4.9. The values show a large dispersion, especially for 60 °C of 5 minutes pressure holding time, which can be seen due to the value greater than 1 for coefficient of variation, which means the standard deviation is higher than the mean value.
The large dispersion results from the assumed crack length for not measureable devices. For some samples, the bonded parts fell appart immediately and the crack length could not be measured, but was set to the maximum value, 7cm, the length of the plates. The values for lower temperatures are quite similar but there is

Table 4.3: Calculated bond strength for different pressure holding times, where NS stands for not significant.

		Pressure Holding Time		
Bonding Temperature	**Statistical Characteristic**	**5 min**	**10 min**	**p-value (t-test)**
60 °C	median[J/m^2]	0.076	0.951	data (5 min) not normally distributed
	CV	2.228	0.633	
65 °C	median[J/m^2]	1.372	5.109	data (5 min) not normally distributed
	CV	0.618	0.296	
70 °C	median[J/m^2]	8.103	11.671	p = NS
	CV	0.384	0.510	
75 °C	median[J/m^2]	47.012	37.470	p = NS
	CV	0.399	0.580	
80 °C	median[J/m^2]	186.528	445.387	p = NS
	CV	0.603	0.765	

an increase of bond strength at 80 °C. To check the distribution of the data, the Shapiro-Wilk-Test was performed on the data for 10 minutes pressure holding time. The results showed a p-value higher than 0.05 for every temperature. It can be assumed that the data are normally distributed. As mentioned above, the data for 5 minutes pressure holding time can be assumed as normally distributed for 70 °C, 75 °C and 80 °C. Again the data for higher tempertures ($\geq$ 70 °C) were tested to show whether the difference is significant by using the t-test. The results show that there is no significant difference between the mean values of the data for 70 °C and 75 °C. For the different pressure holding times of 80 °C a significant difference can be assumed. However, the performed t-test is not valid in this case because the homogeneity of the variances is not sure, which was tested by the f-test. Due to this, the welch-test had to be performed for 80 °C, which not indicated a significant difference between the values of the pressure holding times of 5 and 10 minutes. The performance of these statistic tests should be considered as restricted due to the small amount of samples.

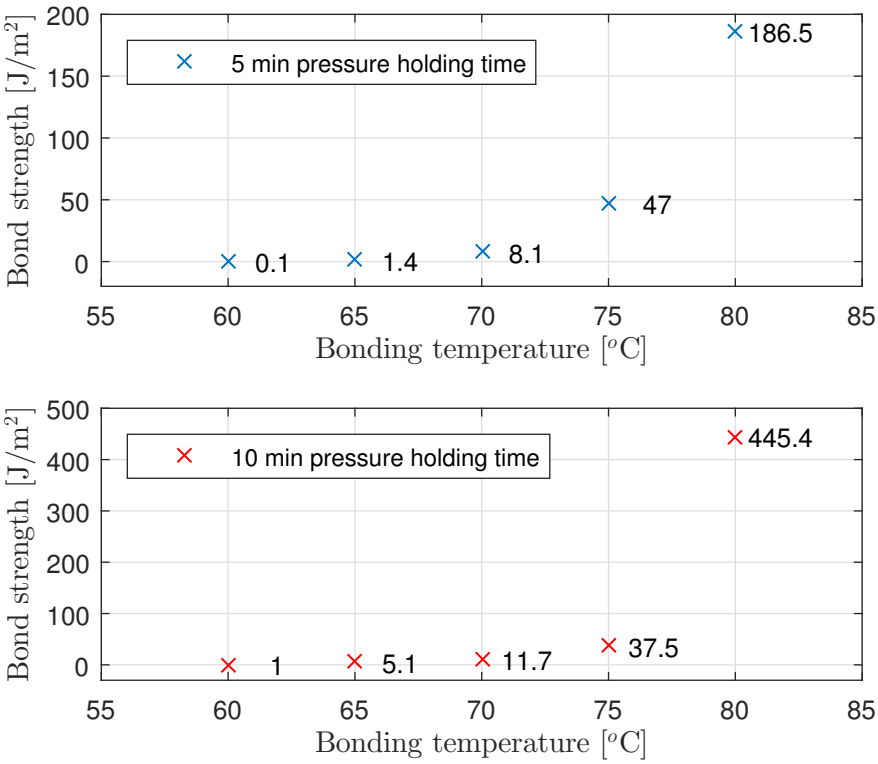

Figure 4.9: Comparison of different pressure holding times.

4.2.2.3 Homogenization of Membrane Plate

In the previous calculations and results, the fact of two component injection molded membrane plate was neglected and only the Young's modulus of COC as non-elastomeric material was taken into account. To examine the difference between the Young's moduli of the homogenized material and of the COC alone, the equation of the book of Bonnet [8] was used.
The equation to calculate the effective stiffness $\bar{E}$ for a tensile load, they presented as following,

$$\bar{E} = \alpha \cdot E_1 + (1 - \alpha) \cdot E_2, \tag{4.6}$$

where E_1 and E_2 are the Young's moduli of the two materials, COC and eCOC, and α is the proportion of thickness of the material. The thicknesses of the materials presented in Section 3.1 were standardized and inserted into the equation. The values for the Young's moduli are cited in Table 3.1.

$$\bar{E} = \frac{7}{12} \cdot 2600 \text{ MPa} + (1 - \frac{7}{12}) \cdot 50 \text{ MPa} = 1537.5 \text{ MPa} \tag{4.7}$$

The results of bond strengths were calculated again using the $\bar{E}$ as Young's modulus for the membrane plate.

$$\gamma = \frac{3 \cdot t_b^2 \cdot E_1 \cdot t_{s1}^3 \cdot \bar{E} \cdot t_{s2}^3}{16 \cdot L^4 \cdot (E_1 \cdot t_{s1}^3 + \bar{E} \cdot t_{s2}^3)} \tag{4.8}$$

The calculation example in Equation 4.5 is repeated for the new Young's modulus for the membrane plate.

$$\gamma = \frac{3 \cdot (0.38 \text{ mm})^2 \cdot 2600 \text{ MPa} \cdot (1.5 \text{ mm})^3 \cdot 1537.5 \text{ MPa} \cdot (1.2 \text{ mm})^3}{16 \cdot (7.95 \text{ mm})^4 \cdot (2600 \text{ MPa} \cdot (1.5 \text{ mm})^3 + 1537.5 \text{ MPa} \cdot (1.2 \text{ mm})^3)} \tag{4.9}$$

$$\gamma = 13.84 \frac{\text{J}}{\text{m}^2} \tag{4.10}$$

The diagrams in Figure 4.10 show the differences of the calculated bond strengths

(median, N=4 for 0 min UV/ozone exposure, M=8 for 10 min UV/ozone exposure prior to bonding) by using the Young's modulus for the homogenized material of membrane plate compared to the results of the bond strengths where only the Young's modulus of the COC component was taken into consideration and the elastomeric component was neglected. In both cases, for 10 minutes UV/ozone pretreatment and for substrates without prior modification, the results show much higher bond strengths for the homogenized cases. That can be explained by the material thickness of the homogenized membrane plate. The Young's modulus of the homogenized material is about 1000 MPa smaller than that of COC alone. However, the thickness of the material for the calculation of the bond strength with the homogenized membrane plate is 1.2 mm, the thicknesses of COC and eCOC. For the calculation without considering the elastomeric component, only the thickness of the COC was used for the calculation.

The data were again examined using R. It can not be shown that the data for 60 °C and 65 °C are normally distributed for 0 minutes of exposure, as well as for 10 minutes exposure. To determine whether the difference between the results of the homogenized and the non-homogenized values is significant for the normally distributed data, the t-test was performed. For 10 minutes exposure time, the values for homogenized and non-homogenized materials are significantly ($p < 0.05$) different for temperatures of 75 °C and 80 °C. For 70 °C no significant ($p = NS$) difference of the mean values can be shown. For the measurements without prior UV/ozone treatment, it can be shown that the values for homogenized and non-homogenized materials indicate no significant ($p = NS$) difference for temperatures higher than 65 °C.

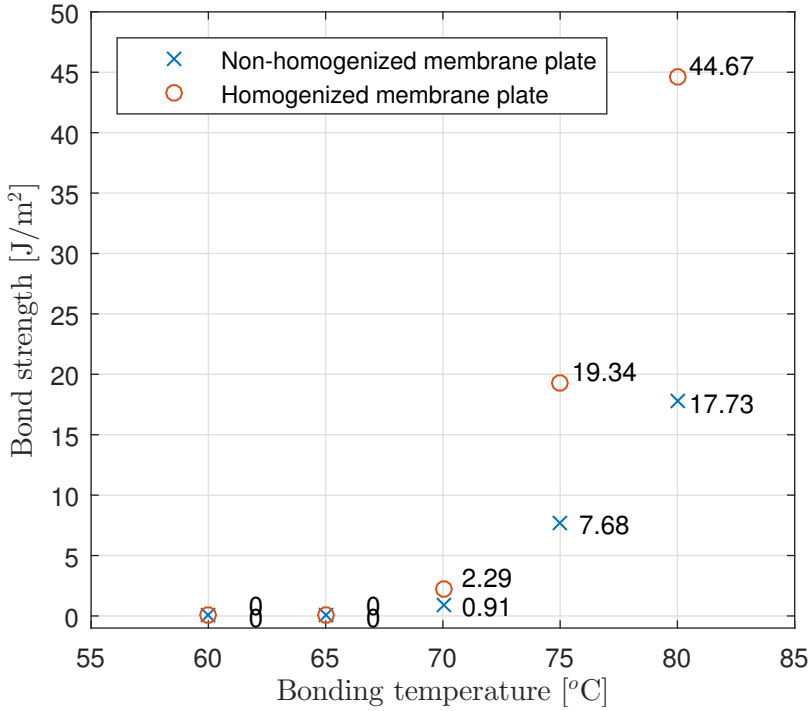

(a) No UV/ozone exposure prior to bonding

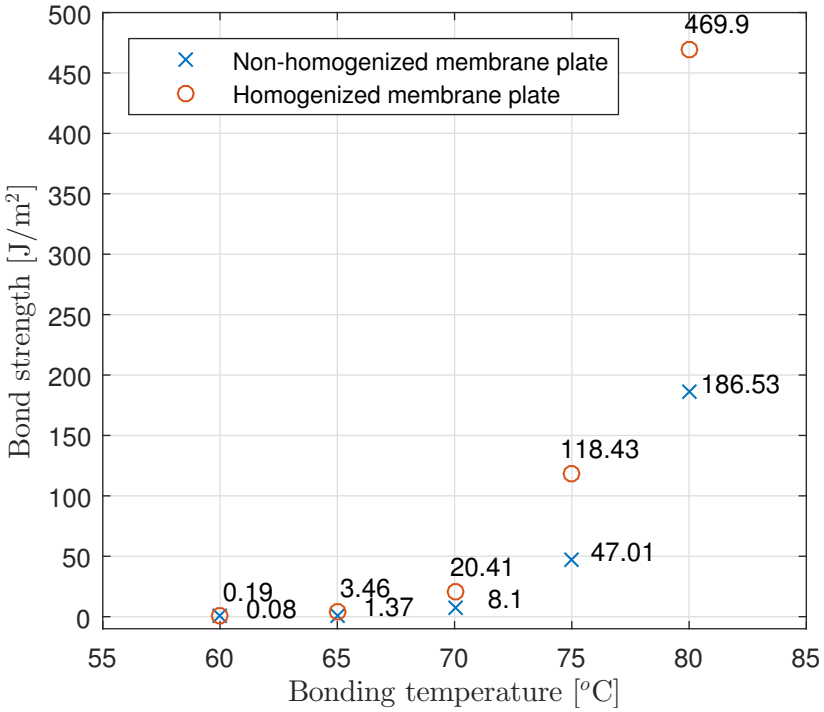

(b) 10 min UV/ozone exposure time

Figure 4.10: Comparison of calculated bond strengths for Young's modulus of membrane plate homogenized and non-homogenized. (a) Results without UV/ozone exposure prior to bonding. (b) Results with 10 minutes UV/ozone exposure prior to bonding

Chapter 5

Discussion

In summary, the results show an improvement of bond strength with UV/ozone pretreatment compared to without surface modification. The parameter with major influence is the bonding temperature, because at lower temperatures of 60 °C, the effect of UV/ozone is not enough to achieve a good bonding quality. The higher the bonding temperature the higher the bond strength.

Contact Angle Measurements

Due to the curvature of the elastomeric membrane plate, the measurements of the contact angles were tricky. The measurements can be optimized by finding a clamping method to attach the substrate flat on the table of the measuring instrument and hence improve the results. A special cleaning of the polymeric substrates before the measurements is another possible improvement of the contact angle measurements. Due to handling, the surface of the substrate may be greasy or dust particles may settle on the surface. The unexpected increase of the contact angle between 10 minutes and 20 minutes exposure time of the base plate, which can be seen in Figure 4.2, is perhaps an indication of an unclean surface. An appropriate solution for this possible influence on the measurements is cleaning the substrates with isopropanol or another alcohol, and drying it in a drying cabinet afterwards. The T_g has to be taken under consideration, because of deformation of the plates in the drying cabinet in case of higher temperatures. Figure 4.2 shows the interesting fact that the contact angles for the cover part are lower for each duration of exposure.

Therefore, the wettability of the eCOC is always higher compared to the COC. Because eCOC is a quite new material, there was no information about the contact angles found in literature. But the results suggest that the elastomeric component is responsible for the higher wettability.

Burst Pressure Test

The burst pressure test is often found in literature to identify the bond strength. However, this technique needs improvement, as in case of detection of the leak. The difficulty is that a leak occurs very quickly, especially for such small bonding areas, as presented in Section 3.4.1.1. If there are dust inclusions, for example, the bond could be very strong but leaky in one specific location, which makes the test very unreliable. The acoustic perception of the leaks is a subjective, uncertain factor. The burst pressure test can be improved by measuring the pressure drop, if it is detectable and a wider circular bonding area could compensate the leaks due to dust inclusions. A cleaning step would also improve the quality of the bonded area. It has to be taken under consideration that the cleaning process has to be done before the UV/ozone exposure and not afterwards, in order not to affect the modified surfaces by isopropanol or another alcohol. Alternatives to the cleaning process is the infrastructure of a cleanroom or an antistatic treatment of the polymer parts prior UV/ozone exposure.

Wedge Test

The wedge test method is a subjective method to determine the bond strength. So the results are hard to compare to results in literature but among themselves. The comparison between the results of Tsao *et al.* presented in Section 4.2.2 and the results presented in this research showed, that rinsing the UV/ozone exposed samples in 2-propanol and left them in a vacuum oven for two hours, might be the reason for much lower bond strength.
Several other research groups, like Bhattacharyya *et al.* [28], Gu *et al.* [20] or Zhu *et al.* [46], determined the bond stength using three-point bending tests or tensile tests. Therefore, these groups achieve results of a mechanical tension with the unit Pa. To make them comparable with the results presented in this thesis, a tensile

test would be more meaningful and is a more accurate procedure to determine the force needed to crack the bonded parts apart.
The results of the performed wedge test showed a significant difference between the 10 minutes UV/ozone exposed bond strengths and the non-exposed bond strengths. This indicates that with lower bonding temperatures and a 10 minutes UV/ozone exposure, the same bond strengths can be achieved as with higher temperatures without UV/ozone pretreatment. The lower temperatures result in a decreased risk of clogging or deforming the channels.

In Figure 5.1, the data of 0 minutes and 10 minutes exposure time are shown. The dashed curves are exponential fitting functions to give an idea of the trend of the values. For 0 minutes exposure time prior to bonding, the data fits to the equation given by,

$$f(T) = 1.108 \cdot 10^{-6} \cdot e^{0.2075 \cdot T}, \tag{5.1}$$

where T is the temperature. The fit shows a regression coefficient of,

$$R^2 = 0.9817. \tag{5.2}$$

The regression coefficient indicates how good a model describes the amount of collected data. The closer R^2 is to one, the better is the fitting between the calculated values for the bond strength and the fitting curve.

For 10 minutes of exposure, the data also fit to an exponential equation given by,

$$f(T) = 2.722 \cdot 10^{-8} \cdot e^{0.2831 \cdot T}, \tag{5.3}$$

where T is the temperature and with the coefficient of regression is given by,

$$R^2 = 0.9995. \tag{5.4}$$

The fitting curves were determined by MATLAB®. A polynomial function was also expected as a fitting curve, but there could be values of bond strength smaller than zero, which was considered as a incorrect fitting.

As discussed in Section 4.2.2, the difference between 5 and 10 minutes pressure holding time is not significant. Therefore, the time-saving aspect is in the foreground and the substrates can be bonded with 5 minutes pressure holding time.
The homogenization of the membrane plate shows an increase of the resulting bond strengths for each temperature for substrates exposed for 10 minutes. The fact of two different Young's moduli of the membrane plate should be considered. The first assumption that the Young's modulus of the eCOC has minor influence shows much lower bond strengths. The stiffness of the COC is much higher than that of the eCOC and so the total stiffness of the membrane plate is lower than that of COC alone.
There is one important aspect to consider for the homogenization of the Young's modulus of the two-component membrane plate. The calculation of the Young's modulus for the combined material presented in Section 4.2.2, is only valid for loads parallel to bonding interface. In case of wedge test, the load is not parallel to the interface but much more a bending load. An approach for combined materials loaded with a bend could achieve more accurate results, but the results presented in this research give an idea of the influence of the thicknesses and the Young's modulus of the material on the calculated bond strengths.

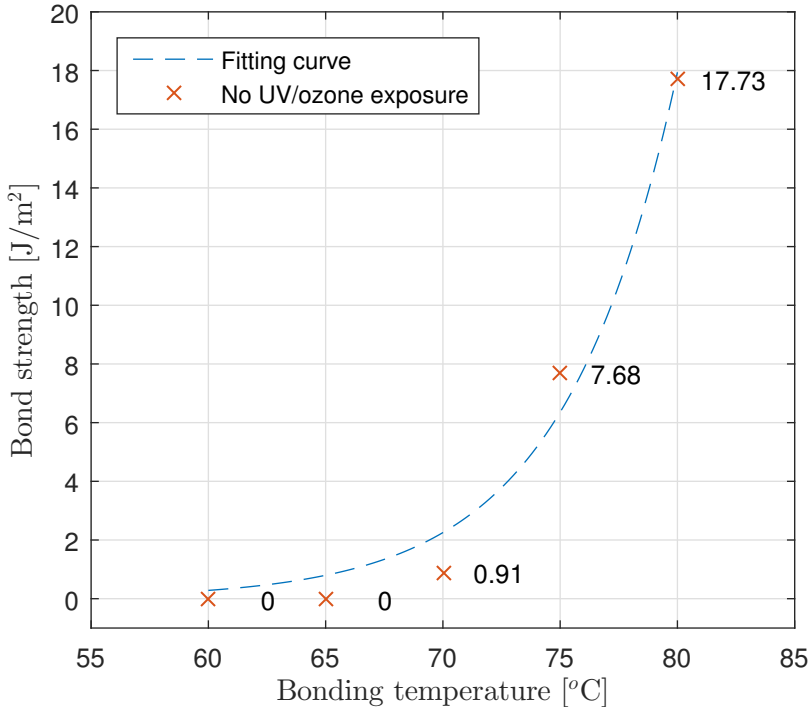

(a) Fitting curve for non-exposed parts

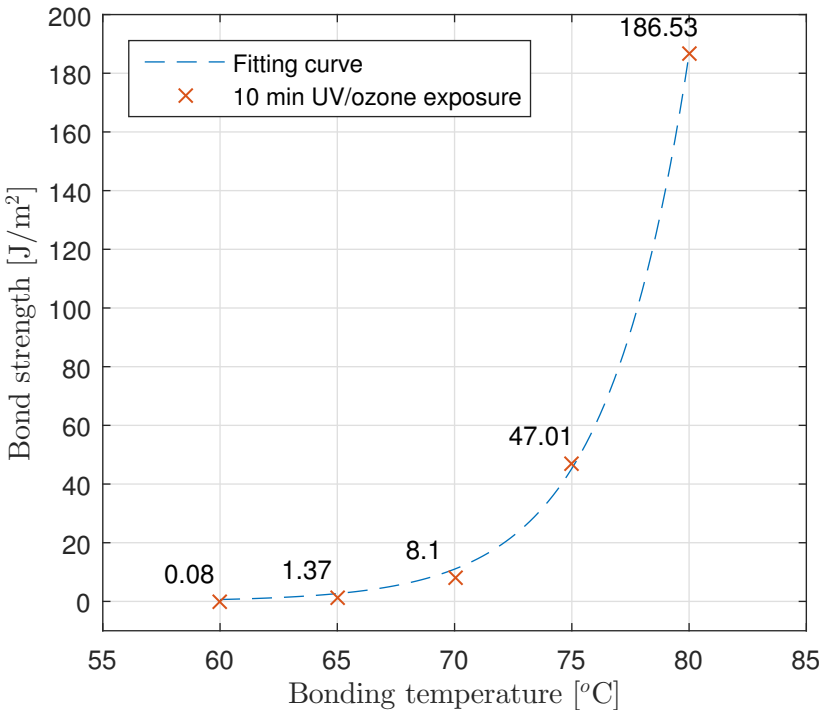

(b) Fitting curve for 10 min UV/ozone exposure time

Figure 5.1: Data of 0 and 10 minutes UV/ozone exposed microfluidic devices. The dotted lines represent exponential fitting curves. (a) Results and fitting curve for non-exposed plates. (b) Results and fitting curve for 10 minutes UV/ozone exposed plates.

Chapter 6

Conclusion

The contact angle measurements, as a first investigation of the surface properties, showed an increasing hydrophilicity for increasing time of UV/ozone irradiation. The eCOC always showed a better wettability compared to the COC, which indicates the lower contact angles. The negative slope of the contact angles decreased rapidly after the first 5 minutes of UV/ozone exposure.
The second method for the investigation of the surface by ATR-IR spectroscopy indicated the presence of oxygen-based functionalities, which facilitate a reliable bonding quality. It further showed an increase of the functional groups by increasing exposure time. Based on the results of the methods to characterize the surface after the UV/ozone examination of the polymer plates, adequate conditions for reliable bonding could be determined.
The combination of a microfluidic COC and the two component injection molded lid of COC and the quite new elastomeric polymer eCOC can achieve quite good bonding qualities and a high bond strength by supportive UV/ozone surface activation prior to bonding. The bonding experiments have shown a higher bond strength for increasing temperatures. Statistical investigation pointed out a significant difference in bond strength between non-exposed and 10 minutes exposed thermocompression bonded polymer plates. There was no significant difference in bond strength between 5 and 10 minutes pressure holding time. Therefore, the conclusion can be made that bonding temperature is the most important bonding parameter after the best duration of UV/ozone modification was chosen.
For the two component membrane plate, a homogenization calculation for the Young's

modulus was carried out, which indicated a significant difference of the results. Due to the incompatibility between the data of the carried out wedge test and literature results, it is possible to calculate the bond strenghts without the homogenization of the two materials of the membrane plate. In general, an approach for bending loads could achieve more accurate results in case of the performed wedge test.
The major advantages of the thermocompression bonding with UV/ozone pretreatment are the easy implementation and the low costs associated with it. Of course, there are some possible improvements of the measurements, but as a first investigation of eCOC as an elastomeric layer in microfluidic devices for the application for microvalves or other actuators, the results give a good overview of UV/ozone supportive thermocompression bonding.

Bibliography

[1] Roger C Lo. "Microfluidics technology: future prospects for molecular diagnostics". In: *Advanced Health Care Technologies* (2017), p. 17.

[2] N. Nguyen. *Entwurf, Herstellung und Charakterisierung*. B. G. Teubner Verlag, 2004.

[3] K. V. Sharp et al. "Liquid Flows in Microchannels". In: *The MEMS Handbook*. 2005. Chap. 10, p. 48.

[4] C.W. Tsao and D.L. DeVoe. "Bonding of thermoplastic polymer microfluidics". In: *Microfluidics and Nanofluidics* (2009), pp. 1–16.

[5] E. Wintermantel. *Medizintechnik*. Berlin Heidelberg Springer Verlag, 2009.

[6] C.W. Tsao. "Polymer microfluidics: Simple, low-cost fabrication process bridging academic lab research to commercialized production". In: *Micromachines* (2016), p. 11.

[7] T Brown and T. Jr. Brown. *Solid-phase oligonucleotide synthesis*. URL: `https://www.atdbio.com/content/17/Solid-phase-oligonucleotide-synthesis{\#}Advantages-of-solid-phase-synthesis` (visited on 05/22/2018).

[8] M. Bonnet. *Kunststoffe in der Ingenieuranwendung*. Vieweg+Teubner, 2009.

[9] H. Domininghaus. *Kunststoffe*. Berlin Heidelberg Springer Verlag, 2008.

[10] R. Ziel. *Schematic Arrangement of Molecular Chains in Amorphous and Semicrystalline Polymers*. 2010. URL: `https://commons.wikimedia.org/wiki/File:Polymerketten{\_}-{\_}amorph{\_}und{\_}kristallinEN.svg` (visited on 06/14/2018).

[11] W.I. Wu et al. "Materials and methods for the microfabrication of microfluidic biomedical devices". In: *Microfluidic Devices for Biomedical Applications*. Woodhead Publishing Limited, 2013. Chap. 1, pp. 3–62.

[12] F. Namouchi et al. "Thermally stimulated depolarization current and dielectric spectroscopy used to study dipolar relaxations and trap level distribution in PMMA polymer". In: *Journal of Non-Crystalline Solids* (2015), pp. 76–82.

[13] P.S. Nunes et al. "Cyclic olefin polymers: Emerging materials for lab-on-a-chip applications". In: *Microfluidics and Nanofluidics* (2010).

[14] R.O. Rodrigues et al. "Polymer microfluidic devices: an overview of fabrication methods". In: *U.Porto Journal of Engineering* (2015), pp. 67–79.

[15] S. Miserere et al. "Fabrication of thermoplastics chips through lamination based techniques". In: *Lab on a Chip* (2012), pp. 1849–1856.

[16] U.M. Attia et al. "Micro-Injection Moulding of Polymer Microfluidic Devices". In: *Microfluidics and Nanofluidics* (2009), pp. 1–28.

[17] L. Riegger et al. "Adhesive bonding of microfluidic chips : influence of process parameters". In: *J . Micromech . Microeng . J . Micromech . Microeng* (2010), p. 5.

[18] Y. Temiz et al. "Lab-on-a-chip devices: How to close and plug the lab?" In: *Microelectronic Engineering* (2015), pp. 156–175.

[19] C.W. Tsao et al. "Low temperature bonding of PMMA and COC microfluidic substrates using UV/ozone surface treatment". In: *Lab on a Chip* (2007), pp. 499–505.

[20] Pan Gu et al. "Chemical-assisted bonding of thermoplastics/elastomer for fabricating microfluidic valves". In: *Analytical Chemistry* 83.1 (2011), pp. 446–452.

[21] I .R.G. Ogilvie et al. "Reduction of surface roughness for optical quality microfluidic devices in PMMA and COC". In: *Journal of Micromechanics and Microengineering* (2010), p. 8.

[22] S. Herrlich et al. "Solvent Bonding of a Drug Delivery Device by Using Hansen Solubility Parameters". In: *Proceedings of the 8th International Conference on Multi-Material Micro Manufacture* (2011), pp. 38–41.

[23] S. H. Ng et al. "Thermally activated solvent bonding of polymers". In: *Microsystem Technologies* (2008), pp. 753–759.

[24] A.M.D. Wan et al. "Liquid phase solvent bonding of plastic microfluidic devices assisted by retention grooves". In: *Lab Chip* (2015), p. 20.

[25] D. Ogończyk et al. "Bonding of microfluidic devices fabricated in polycarbonate". In: *Lab on a Chip* (2010), pp. 1324–1327.

[26] S. Roy et al. "Surface analysis, hydrophilic enhancement, ageing behavior and flow in plasma modified cyclic olefin copolymer (COC)-based microfluidic devices". In: *Sensors and Actuators, B: Chemical* (2010), pp. 537–549.

[27] P.M. van Midwoud et al. "Comparison of Biocompatibility and Adsorption Properties of Different Plastics for Advanced Microfluidic Cell and Tissue Culture Models". In: *Analytical Chemistry* (2012), pp. 3938–3944.

[28] A. Bhattacharyya and C.M. Klapperich. "Mechanical and chemical analysis of plasma and ultraviolet ozone surface treatments for thermal bonding of polymeric microfluidic devices". In: *Lab Chip* (2007), pp. 876–882.

[29] J.R. Vig. "UV/ozone cleaning of surfaces". In: *J. Vac. Sci. Technol.* (1985).

[30] B.W. Callen et al. "Remote plasma and ultravioletâĂŞozone modification of polystyrene". In: *Journal of Vacuum Science & Technology A: Vacuum, Surfaces, and Films* 13.4 (1995), pp. 2023–2029.

[31] Che Hsin Lin et al. "Low azeotropic solvent for bonding of PMMA microfluidic devices". In: *Sensors and Actuators, B: Chemical* (2007).

[32] Y. Berdichevsky et al. "UV/ozone modification of poly(dimethylsiloxane) microfluidic channels". In: *Sensors and Actuators, B: Chemical* (2004), pp. 402–408.

[33] Y. Luo et al. "Ultrasonic bonding for thermoplastic microfluidic devices without energy director". In: *Microelectronic Engineering* (2010), pp. 2429–2436.

[34] K. Kistrup et al. "Ultrasonic welding for fast bonding of self-aligned structures in lab-on-a-chip systems". In: *Lab Chip* (2015), pp. 1998–2001.

[35] K. Kistrup et al. "Fabrication and modelling of injection moulded all-polymer capillary microvalves for passive microfluidic control". In: *Journal of Micromechanics and Microengineering* (2014), p. 10.

[36] F. Dang et al. "Replica multichannel polymer chips with a network of sacrificial channels sealed by adhesive printing method". In: *Lab on a Chip* 5 (2005), pp. 472–478.

[37] S. Abbott. *Adhesion Science: Principles and Practice*. Lancaster, 2015, p. 299.

[38] N. Keller et al. "Tacky cyclic olefin copolymer: a biocompatible bonding technique for the fabrication of microfluidic channels in COC". In: *Lab Chip* (2016), pp. 1561–1564.

[39] M. Wiemer et al. "Plasma - Activated Bonding". In: *Handbook of Wafer Bonding*. 2012, pp. 101–117.

[40] S. Roy et al. "Thermal bonding of microfluidic devices: Factors that affect interfacial strength of similar and dissimilar cyclic olefin copolymers". In: *Sensors and Actuators, B: Chemical* (2012).

[41] V. Bürgin et al. "90 Degree Peel off Tests of Tissue Engineered Osteochondral Constructs: A New Method to Determine the Osteochondral Integration". In: *International Journal of Tissue Engineering* (2014), p. 6.

[42] W.P. Maszara et al. "Bonding of silicon wafers for silicon-on-insulator". In: *Journal of Applied Physics* 64.10 (1988), pp. 4943–4950.

[43] *Technical Data Sheet - COC*. URL: `https://topas.com/sites/default/files/TDS{\_}8007S-04{\_}e{\_}EU.pdf` (visited on 08/15/2018).

[44] *Technical Data Sheet - eCOC*. URL: `https://topas.com/sites/default/files/TDS{\_}ElastomerE-140{\_}e{\_}EU.pdf` (visited on 08/15/2018).

[45] Y Yuan and T.R. Lee. "Contact Angle and Wetting Properties". In: *Surface Science Techniques*. Vol. 51. 1. Springer-Verlag Berlin Heidelberg, 2010. Chap. 1, p. 34.

[46] X. Zhu et al. "Study of PMMA thermal bonding". In: *Microsystem Technologies* (2007).

Attachment

1. Matlab Code

a) Contact Angle Measurement

```
%Set font size for axes and text
set(0,'defaultAxesFontSize',10)
set(0,'defaultTextFontSize',10)

%Read in the data of contact angles
c_ang = dlmread('U:\Diplomarbeit Latex\Data\contact
   angles for different exposure times_mean.csv', ';');
c_ang_std_dev = dlmread('U:\Diplomarbeit Latex\Data\
   contact angles for different exposure times_std_dev.
   csv', ';');

c_ang_base = c_ang(:,1);
c_ang_membrane = c_ang(:,2);
c_ang_base_std_dev = c_ang_std_dev(:,1);
c_ang_membrane_std_dev = c_ang_std_dev(:,2);

%Duration of exposure
dur_exp = [0,5,10,20];
std(c_ang_base, dur_exp)

```

```
%Plot of contact angles of base plate (COC) and membrane plate (eCOC)
figure('Units', 'centimeters', 'Position', [40 10 10 8], ...
    'PaperUnits', 'centimeters', 'PaperSize',[12 10], 'PaperPosition', [0 0 12 10])
%plot(dur_exp, c_ang_base,  'x', dur_exp, c_ang_membrane, 'o'); grid
%hold on;
errorbar(dur_exp, c_ang_base, c_ang_base_std_dev, 'x', 'MarkerEdgeColor','blue');grid
hold on;
errorbar(dur_exp, c_ang_membrane, c_ang_membrane_std_dev, 'o', 'MarkerEdgeColor','red')
xlabel('Duration of exposure [min]', 'Interpreter', 'latex'),...
    ylabel('Contact angle [$^{o}$]', 'Interpreter', 'latex'),...
    legend('Base plate','Membrane plate','Interpreter', 'latex'),
axis([0 25 0 95])
values_base = num2str(round(c_ang_base,1));
values_membrane = num2str(round(c_ang_membrane,1));
txt_base = cellstr(values_base);
txt_membrane = cellstr(values_membrane);
text(dur_exp+0.5, c_ang_base+2, txt_base),text(dur_exp+0.5, c_ang_membrane-1, txt_membrane);
print('U:\Diplomarbeit Latex\Figs\contact_angles','-depsc')
print('U:\Bonding Technologies\Diplomarbeit\zweite Teilpräsentation\contact_angles','-djpeg')
```

b) IR-Spectroscopy

```
%Set font size for axes and text
set(0,'defaultAxesFontSize',10)
set(0,'defaultTextFontSize',10)

%COC 2min UV/ozone different positions on one sample
figure('Units', 'centimeters', 'Position', [40 10 10 8],
   ...
    'PaperUnits', 'centimeters', 'PaperSize',[9 8], '
       PaperPosition', [0 0 9 8])
COC_02min_Pos01 = plot(COC_02min04_Pos01(:,1),
   COC_02min04_Pos01(:,2)); grid
set(gca,'XDir','reverse');
hold on;
COC_02min_Pos02 = plot(COC_02min04_Pos02(:,1),
   COC_02min04_Pos02(:,2))
set(gca,'XDir','reverse');
hold on;
COC_02min_Pos03 = plot(COC_02min04_Pos03(:,1),
   COC_02min04_Pos03(:,2))
set(gca,'XDir','reverse');
hold on;
COC_02min_Pos04 = plot(COC_02min04_Pos04(:,1),
   COC_02min04_Pos04(:,2))
set(gca,'XDir','reverse');
hold on;
COC_02min_Pos05 = plot(COC_02min04_Pos05(:,1),
   COC_02min04_Pos05(:,2))
set(gca,'XDir','reverse');
hold on;
COC_02min_Pos06 = plot(COC_02min04_Pos06(:,1),
   COC_02min04_Pos06(:,2))
set(gca,'XDir','reverse');
hold on;
set(gca,'XDir','reverse');
```

```
27 xlabel('Wavenumber [cm$^{-1}$]', 'Interpreter', 'latex'),
      ...
28     ylabel('Transmittance [\%T]', 'Interpreter', 'latex')
29 xlim([600 4000])
30 ylim([0.975 1.006])
31 legend([COC_02min_Pos01, COC_02min_Pos02, COC_02min_Pos03
      , COC_02min_Pos04, COC_02min_Pos05, COC_02min_Pos06],
      ...
32 {'Pos01', 'Pos02','Pos03','Pos04','Pos05','Pos06'},'
      Location','SouthEast', 'Interpreter', 'latex','
      FontSize',8)
33 hold off;
34 print('U:\Diplomarbeit Latex\Figs\
      IR_spectroscopy_COC_2min_diff_pos','-depsc')
35 print('U:\Diplomarbeit Latex\Figs\
      IR_spectroscopy_COC_2min_diff_pos','-djpeg')
36
37 %COC 2min UV/ozone different positions on one sample
38 figure('Units', 'centimeters', 'Position', [40 10 10 8],
      ...
39     'PaperUnits', 'centimeters', 'PaperSize',[6 8], '
         PaperPosition', [0 0 6 8])
40 COC_02min_Pos01 = plot(COC_02min04_Pos01(:,1),
      COC_02min04_Pos01(:,2)); grid
41 set(gca,'XDir','reverse');
42 hold on;
43 COC_02min_Pos02 = plot(COC_02min04_Pos02(:,1),
      COC_02min04_Pos02(:,2))
44 set(gca,'XDir','reverse');
45 hold on;
46 COC_02min_Pos03 = plot(COC_02min04_Pos03(:,1),
      COC_02min04_Pos03(:,2))
47 set(gca,'XDir','reverse');
48 hold on;
```

```
49 COC_02min_Pos04 = plot(COC_02min04_Pos04(:,1),
      COC_02min04_Pos04(:,2))
50 set(gca,'XDir','reverse');
51 hold on;
52 COC_02min_Pos05 = plot(COC_02min04_Pos05(:,1),
      COC_02min04_Pos05(:,2))
53 set(gca,'XDir','reverse');
54 hold on;
55 COC_02min_Pos06 = plot(COC_02min04_Pos06(:,1),
      COC_02min04_Pos06(:,2))
56 set(gca,'XDir','reverse');
57 hold on;
58 set(gca,'XDir','reverse');
59 xlabel('Wavenumber [cm$^{-1}$]', 'Interpreter', 'latex'),
      ...
60     ylabel('Transmittance [\%T]', 'Interpreter', 'latex')
61 xlim([1500 1800])
62 hold off;
63 print('U:\Diplomarbeit Latex\Figs\
      IR_spectroscopy_COC_2min_diff_pos_detail','-depsc')
64 print('U:\Diplomarbeit Latex\Figs\
      IR_spectroscopy_COC_2min_diff_pos_detail','-djpeg')
65
66 %COC comparison different exposure times
67 figure('Units', 'centimeters', 'Position', [40 10 10 8],
      ...
68     'PaperUnits', 'centimeters', 'PaperSize',[9 8], '
         PaperPosition', [0 0 9 8])
69 COC_0min = plot(COC_unbeh01_Pos03(:,1),COC_unbeh01_Pos03
      (:,2)); grid
70 set(gca,'XDir','reverse');
71 hold on;
72 COC_01min = plot(COC_01min02_Pos01(:,1),COC_01min02_Pos01
      (:,2))
73 set(gca,'XDir','reverse');
```

```
74 hold on;
75 COC_02min = plot(COC_02min02_Pos01(:,1),COC_02min02_Pos01
      (:,2))
76 set(gca,'XDir','reverse');
77 hold on;
78 COC_05min = plot(COC_05min01_Pos01(:,1),COC_05min01_Pos01
      (:,2))
79 set(gca,'XDir','reverse');
80 hold on;
81 COC_10min = plot(COC_10min01_Pos01(:,1),COC_10min01_Pos01
      (:,2))
82 set(gca,'XDir','reverse');
83 hold on;
84 COC_15min = plot(COC_15min01_Pos01(:,1),COC_15min01_Pos01
      (:,2))
85 set(gca,'XDir','reverse');
86 hold on;
87 COC_20min = plot(COC_20min01_Pos01(:,1),COC_20min01_Pos01
      (:,2))
88 set(gca,'XDir','reverse');
89 hold on;
90 set(gca,'XDir','reverse');
91 xlabel('Wave number [cm$^{-1}$]', 'Interpreter', 'latex')
      ,...
92     ylabel('Transmittance [\%T]', 'Interpreter', 'latex')
93 xlim([600 4000])
94 legend([COC_0min, COC_01min, COC_02min, COC_05min,
      COC_10min, COC_15min, COC_20min],...
95 {'Untreated', '01 min','02 min','05 min','10 min','15 min
      ','20 min'},'Location','SouthEast', 'Interpreter', '
      latex','FontSize',8)
96 hold off;
97 print('U:\Diplomarbeit Latex\Figs\
      IR_spectroscopy_COC_diff_exp_times','-depsc')
```

```
98  print('U:\Diplomarbeit Latex\Figs\
       IR_spectroscopy_COC_diff_exp_times','-djpeg')
99
100 %COC comparison different exposure times
101 figure('Units', 'centimeters', 'Position', [40 10 10 8],
       ...
102     'PaperUnits', 'centimeters', 'PaperSize',[6 8], '
          PaperPosition', [0 0 6 8])
103 COC_0min = plot(COC_unbeh01_Pos03(:,1),COC_unbeh01_Pos03
       (:,2)); grid
104 set(gca,'XDir','reverse');
105 hold on;
106 COC_01min = plot(COC_01min02_Pos01(:,1),COC_01min02_Pos01
       (:,2))
107 set(gca,'XDir','reverse');
108 hold on;
109 COC_02min = plot(COC_02min02_Pos01(:,1),COC_02min02_Pos01
       (:,2))
110 set(gca,'XDir','reverse');
111 hold on;
112 COC_05min = plot(COC_05min01_Pos01(:,1),COC_05min01_Pos01
       (:,2))
113 set(gca,'XDir','reverse');
114 hold on;
115 COC_10min = plot(COC_10min01_Pos01(:,1),COC_10min01_Pos01
       (:,2))
116 set(gca,'XDir','reverse');
117 hold on;
118 COC_15min = plot(COC_15min01_Pos01(:,1),COC_15min01_Pos01
       (:,2))
119 set(gca,'XDir','reverse');
120 hold on;
121 COC_20min = plot(COC_20min01_Pos01(:,1),COC_20min01_Pos01
       (:,2))
122 set(gca,'XDir','reverse');
```

```
hold on;
set(gca,'XDir','reverse');
xlabel('Wave number [cm$^{-1}$]', 'Interpreter', 'latex')
   ,...
    ylabel('Transmittance [\%T]', 'Interpreter', 'latex')
xlim([1500 1800])
hold off;
print('U:\Diplomarbeit Latex\Figs\
   IR_spectroscopy_COC_diff_exp_times_detail','-depsc')
print('U:\Diplomarbeit Latex\Figs\
   IR_spectroscopy_COC_diff_exp_times_detail','-djpeg')
```

```
%Set font size for axes and text
set(0,'defaultAxesFontSize',10)
set(0,'defaultTextFontSize',10)

%eCOC 15min UV/ozone different positions on one sample
figure('Units', 'centimeters', 'Position', [40 10 10 8],
   ...
    'PaperUnits', 'centimeters', 'PaperSize',[13 10], '
       PaperPosition', [0 0 13 10])
eCOC_15min_Pos01 = plot(eCOC_15min04_Pos01(:,1),
   eCOC_15min04_Pos01(:,2)); grid
set(gca,'XDir','reverse');
hold on;
eCOC_15min_Pos02 = plot(eCOC_15min04_Pos02(:,1),
   eCOC_15min04_Pos02(:,2))
set(gca,'XDir','reverse');
hold on;
eCOC_15min_Pos03 = plot(eCOC_15min04_Pos03(:,1),
   eCOC_15min04_Pos03(:,2))
set(gca,'XDir','reverse');
hold on;
set(gca,'XDir','reverse');
xlabel('Wavenumber [cm$^{-1}$]', 'Interpreter', 'latex'),
```

```
   ...
19      ylabel('Transmittance [\%T]', 'Interpreter', 'latex')
20 xlim([600 4000])
21 legend([eCOC_15min_Pos01, eCOC_15min_Pos02,
   eCOC_15min_Pos03],...
22 {'Pos01', 'Pos02','Pos03'},'Location','SouthEast', '
   Interpreter', 'latex','FontSize',8)
23 hold off;
24 print('U:\Diplomarbeit Latex\Figs\
   IR_spectroscopy_eCOC_15min_diff_pos','-depsc')
25 print('U:\Diplomarbeit Latex\Figs\
   IR_spectroscopy_eCOC_15min_diff_pos','-djpeg')
26
27 %eCOC comparison different exposure times
28 figure('Units', 'centimeters', 'Position', [40 10 10 8],
   ...
29      'PaperUnits', 'centimeters', 'PaperSize',[13 10], '
          PaperPosition', [0 0 13 10])
30 backgrd = plot(backgrd_2(:,1),backgrd_2(:,2))
31 set(gca,'XDir','reverse');
32 hold on;
33 eCOC_0min = plot(eCOC_unbeh01_Pos01(:,1),
   eCOC_unbeh01_Pos01(:,2)); grid
34 set(gca,'XDir','reverse');
35 hold on;
36 eCOC_01min = plot(eCOC_01min01_Pos01(:,1),
   eCOC_01min01_Pos01(:,2))
37 set(gca,'XDir','reverse');
38 hold on;
39 eCOC_02min = plot(eCOC_02min02_Pos01(:,1),
   eCOC_02min02_Pos01(:,2))
40 set(gca,'XDir','reverse');
41 hold on;
42 eCOC_05min = plot(eCOC_05min02_Pos01(:,1),
   eCOC_05min02_Pos01(:,2))
```

```
set(gca,'XDir','reverse');
hold on;
eCOC_10min = plot(eCOC_10min03_Pos01(:,1),
   eCOC_10min03_Pos01(:,2))
set(gca,'XDir','reverse');
hold on;
eCOC_15min = plot(eCOC_15min02_Pos01(:,1),
   eCOC_15min02_Pos01(:,2))
set(gca,'XDir','reverse');
hold on;
eCOC_20min = plot(eCOC_20min01_Pos01(:,1),
   eCOC_20min01_Pos01(:,2))
set(gca,'XDir','reverse');
hold on;
xlabel('Wavenumber [cm$^{-1}$]', 'Interpreter', 'latex'),
   ...
    ylabel('Transmittance [\%T]', 'Interpreter', 'latex')
xlim([600 4000])
legend([backgrd, eCOC_0min, eCOC_01min, eCOC_02min,
   eCOC_05min, eCOC_10min, eCOC_15min, eCOC_20min],...
{'backgrd','untreated', '01 min','02 min','05 min','10
   min','15 min','20 min'},'Location','South', '
   Interpreter', 'latex','FontSize',7.5)
hold off;
print('U:\Diplomarbeit Latex\Figs\
   IR_spectroscopy_eCOC_diff_exp_times','-depsc')
print('U:\Diplomarbeit Latex\Figs\
   IR_spectroscopy_eCOC_diff_exp_times','-djpeg')
```

b) Burst Pressure Test

```
%Set font size for axes and text
set(0,'defaultAxesFontSize',10)
set(0,'defaultTextFontSize',10)
```

```
4
5  %Manual data insert of temp and pressure for burst
       pressure
6  temp_bp = [60,65,70,80];
7  pressure = [8,19,25,29];
8
9  %Plot of burst pressure data
10 figure('Units', 'centimeters', 'Position', [40 10 12 10],
       ...
11     'PaperUnits', 'centimeters', 'PaperSize',[12 10], '
           PaperPosition', [0 0 12 10])
12 plot(temp_bp, pressure,'ro');grid
13 xlabel('Bonding temperature [$^{o}$C]', 'Interpreter', '
       latex'),...
14     ylabel('Burst pressure [kN/m$^2$]', 'Interpreter', '
           latex'),
15 axis([55 86 0 30])
16 val_str = num2str(round(pressure,0)');
17 txt_bp = cellstr(val_str);
18 text(temp_bp+0.5, pressure, txt_bp);
19 print('U:\Diplomarbeit Latex\Figs\burst_pressure_results'
       ,'-depsc')
```

c) Wedge Test

```
1  %Set font size for axes and text
2  set(0,'defaultAxesFontSize',10)
3  set(0,'defaultTextFontSize',10)
4
5  %Read in data calculated data from wedge test, from csv-
       file
6  a = dlmread('0minexposure.csv', ';');
7  b = dlmread('5_min_pressure_time.csv',';');
8  c = dlmread('10_min_pressure_time.csv',';');
```

```
9
10 %Seperate data
11 temp_ = a(:,1);
12 temp = [temp_(1),temp_(5),temp_(9),temp_(13),temp_(17)];
13 data_0min_exp = a(:,2);
14 data_5min_press = b(:,2);
15 data_10min_press = c(:,2);
16
17 data_0min_60C = data_0min_exp(1:4);
18 data_0min_65C = data_0min_exp(5:8);
19 data_0min_70C = data_0min_exp(9:12);
20 data_0min_75C = data_0min_exp(13:16);
21 data_0min_80C = data_0min_exp(17:20);
22
23 data_5min_60C = data_5min_press(1:10);
24 data_5min_65C = data_5min_press(11:20);
25 data_5min_70C = data_5min_press(21:30);
26 data_5min_75C = data_5min_press(31:40);
27 data_5min_80C = data_5min_press(41:50);
28
29 data_10min_60C = data_10min_press(1:8);
30 data_10min_65C = data_10min_press(9:16);
31 data_10min_70C = data_10min_press(17:24);
32 data_10min_75C = data_10min_press(25:32);
33 data_10min_80C = data_10min_press(33:40);
34
35 %Vector with median data of 0 min UV/ozone exposure
36 med_0min = [median(data_0min_60C),median(data_0min_65C),
      median(data_0min_70C),...
37     median(data_0min_75C),median(data_0min_80C)];
38
39 %Vector with median data of 10 min UV/ozone exposure (5
      min pressure
40 %holding time)
```

```
41 med_5min_press = [median(data_5min_60C),median(
      data_5min_65C),...
42     median(data_5min_70C),median(data_5min_75C),median(
          data_5min_80C)];
43
44 %Vector with median data of 10 min pressure holding time
45 med_10min_press = [median(data_10min_60C),median(
      data_10min_65C),...
46     median(data_10min_70C),median(data_10min_75C),median(
          data_10min_80C)];
47
48 %Difference between 0 min UV/ozone exposure and 10 min UV
      /ozone exposure
49 figure('Units', 'centimeters', 'Position', [40 10 10 8],
      ...
50     'PaperUnits', 'centimeters', 'PaperSize',[12 10], '
          PaperPosition', [0 0 12 10])
51 comp_0_10min = plot(temp, med_0min, 'bx', temp,
      med_5min_press, 'ro'); grid
52 hold on;
53 xlabel('Bonding temperature $[^o$C]', 'Interpreter', '
      latex'),...
54     ylabel('Bond strength [J/m$^2$]', 'Interpreter', '
          latex'),
55 legend('No UV/ozone exposure', '10 min UV/ozone exposure'
      , 'Location','NorthWest')
56 axis([55 85 -10 200]);
57 values_7 = num2str(round(med_0min,2)');
58 values_8 = num2str(round(med_5min_press,2)');
59 txt_7 = cellstr(values_7);
60 txt_8 = cellstr(values_8);
61 text(temp+0.5, med_0min, txt_7),text(temp-1.5,
      med_5min_press+9, txt_8);
62 print('U:\Diplomarbeit Latex\Figs\0min_10min_UV_exp','-
      depsc')
```

```
63 print('U:\Bonding Technologies\Diplomarbeit\zweite
      Teilpräsentation\0min_10min_UV_exp','-djpeg')
64
65 %Difference between 5 min and 10 min pressure holding
      time
66 figure('Units', 'centimeters', 'Position', [40 10 10 8],
      ...
67     'PaperUnits', 'centimeters', 'PaperSize',[13 11], '
         PaperPosition', [0 0 13 11])
68 subplot(2,1,1)
69 plot(temp, med_5min_press, 'x');grid
70 xlabel('Bonding temperature $[^o$C]', 'Interpreter', '
      latex'),...
71     ylabel('Bond strength [J/m$^2$]', 'Interpreter', '
         latex'),
72 legend('5 min pressure holding time','Location','
      NorthWest')
73 axis([55 85 -20 200])
74 values_10 = num2str(round(med_5min_press,1)');
75 txt_10 = cellstr(values_10);
76 text(temp+0.5, med_5min_press, txt_10);
77 subplot(2,1,2)
78 plot(temp, med_10min_press, 'xr');grid
79 xlabel('Bonding temperature $[^o$C]', 'Interpreter', '
      latex'),...
80     ylabel('Bond strength [J/m$^2$]', 'Interpreter', '
         latex'),
81 legend('10 min pressure holding time','Location','
      NorthWest')
82 axis([55 85 -30 500]);
83 values_9 = num2str(round(med_10min_press,1)');
84 txt_9 = cellstr(values_9);
85 text(temp+0.5, med_10min_press, txt_9);
86 print('U:\Diplomarbeit Latex\Figs\5
      min_10min_pressure_holding','-depsc')
```

```
87  print('U:\Bonding Technologies\Diplomarbeit\zweite
       Teilpräsentation\5min_10min_pressure_holding','-djpeg'
       )
88
89  %The function for fitting the data of 0 min UV/ozone
       treatment
90  a_fit_0min =   1.108e-06;
91  b_fit_0min =      0.2075;
92  temp_fit = temp(1):(temp(end)-temp(1))/100:temp(end);
93  med_0min_fit = a_fit_0min.*exp(b_fit_0min.*temp_fit);
94  %R^2 = 0.9817
95
96  %Set figure parameter for fitting curve of 0 min exposure
        time
97  figure('Units', 'centimeters', 'Position', [40 10 10 8],
       ...
98      'PaperUnits', 'centimeters', 'PaperSize',[12 10], '
          PaperPosition', [0 0 12 10])
99  fit_curve_0min = plot(temp_fit, med_0min_fit, '--');grid
100 hold on
101 data_0min = plot(temp, med_0min, 'x');
102 hold off
103 xlabel('Bonding temperature $[^o$C]', 'Interpreter', '
       latex'),...
104     ylabel('Bond strength [J/m$^2$]', 'Interpreter', '
          latex'),
105 axis([55 85 -1 20])
106 legend([fit_curve_0min, data_0min],...
107 'Fitting curve', 'No UV/ozone exposure','Location','
       NorthWest', 'Interpreter', 'latex')
108 values_1 = num2str(round(med_0min,2)');
109 txt_1 = cellstr(values_1);
110 text(temp+1, med_0min, txt_1);
111 print('U:\Diplomarbeit Latex\Figs\0min_curve_fitting','-
       depsc')
```

```
112 print('U:\Bonding Technologies\Diplomarbeit\zweite
    Teilpräsentation\0min_curve_fitting','-djpeg')
113
114 %The function for fitting the data of 10 min UV/ozone
    treatment (5 min pressure holding time)
115 a_fit_5min = 2.722e-08;
116 b_fit_5min = 0.2831;
117 med_5min_fit = a_fit_5min.*exp(b_fit_5min.*temp_fit);
118 %R^2 = 0.9995
119
120 %Set figure parameter for fitting curve of 10 min
    exposure time
121 figure('Units', 'centimeters', 'Position', [40 10 10 8],
    ...
122     'PaperUnits', 'centimeters', 'PaperSize',[12 10], '
        PaperPosition', [0 0 12 10])
123 fit_curve_5min = plot(temp_fit, med_5min_fit, '--');
124 hold on
125 data_5min = plot(temp, med_5min_press,'x'); grid
126 hold off
127 xlabel('Bonding temperature $[^o$C]', 'Interpreter', '
    latex'),...
128     ylabel('Bond strength [J/m$^2$]', 'Interpreter', '
        latex'),
129 axis([55 85 -10 200])
130 legend([fit_curve_5min, data_5min],...
131     'Fitting curve', '10 min UV/ozone exposure','Location
        ','NorthWest', 'Interpreter', 'latex')
132 values_2 = num2str(round(med_5min_press,2)');
133 txt_2 = cellstr(values_2);
134 text(temp-3, med_5min_press+10, txt_2);
135 print('U:\Diplomarbeit Latex\Figs\10min_curve_fitting','-
    depsc')
136 print('U:\Bonding Technologies\Diplomarbeit\zweite
    Teilpräsentation\10min_curve_fitting','-djpeg')
```

```
137
138 %Read in homogenized data, check with non-homogenized
       data
139 d = dlmread('0_min_exposure_homogenisiert_1538MPa.csv', '
       ;');
140 e = dlmread('5_min_pressure_time_homogenisiert_1538MPa.
       csv', ';');
141
142 data_0min_homo = d(:,2);
143 data_5min_homo = e(:,2);
144
145 data_0min_60C_homo = data_0min_homo(1:4);
146 data_0min_65C_homo = data_0min_homo(5:8);
147 data_0min_70C_homo = data_0min_homo(9:12);
148 data_0min_75C_homo = data_0min_homo(13:16);
149 data_0min_80C_homo = data_0min_homo(17:20);
150
151 med_0min_homo = [median(data_0min_60C_homo), median(
       data_0min_65C_homo),...
152     median(data_0min_70C_homo), median(data_0min_75C_homo
          ),median(data_0min_80C_homo)];
153
154 data_5min_60C_homo = data_5min_homo(1:10);
155 data_5min_65C_homo = data_5min_homo(11:20);
156 data_5min_70C_homo = data_5min_homo(21:30);
157 data_5min_75C_homo = data_5min_homo(31:40);
158 data_5min_80C_homo = data_5min_homo(41:50);
159
160 med_5min_homo = [median(data_5min_60C_homo), median(
       data_5min_65C_homo),...
161     median(data_5min_70C_homo), median(data_5min_75C_homo
          ), median(data_5min_80C_homo)];
162 median(data_5min_80C_homo)
163 %Plot of 0 min UV/ozone exposure, and 5 min pressure
       holding time,
```

```
%homogenized vs. non-homogenized
figure('Units', 'centimeters', 'Position', [40 10 10 8],...
    'PaperUnits', 'centimeters', 'PaperSize',[12 10], 'PaperPosition', [0 0 12 10])
plot(temp, med_0min, 'x', temp, med_0min_homo, 'o'); grid
xlabel('Bonding temperature $[^o$C]', 'Interpreter', 'latex'),...
    ylabel('Bond strength [J/m$^2$]', 'Interpreter', 'latex'),
legend('Non-homogenized membrane plate', 'Homogenized membrane plate','Location','NorthWest')
axis([55 85 -1 50])
values_3 = num2str(round(med_0min,2)');
values_4 = num2str(round(med_0min_homo,2)');
txt_3 = cellstr(values_3);
txt_4 = cellstr(values_4);
text(temp+0.5, med_0min, txt_3),text(temp+0.5, med_0min_homo+1, txt_4);
print('U:\Diplomarbeit Latex\Figs\0min_UV_homo','-depsc')
print('U:\Bonding Technologies\Diplomarbeit\zweite Teilpräsentation\0min_UV_homo','-djpeg')

%Plot 10 min UV/ozone exposure, and 5 min pressure holding time,
%homogenized vs. non-homogenized
figure('Units', 'centimeters', 'Position', [40 10 10 8],...
    'PaperUnits', 'centimeters', 'PaperSize',[12 10], 'PaperPosition', [0 0 12 10])
plot(temp, med_5min_press, 'x', temp, med_5min_homo, 'o'); grid
xlabel('Bonding temperature $[^o$C]', 'Interpreter', 'latex'),...
```

```
186     ylabel('Bond strength [J/m$^2$]', 'Interpreter', '
           latex'),
187 legend('Non-homogenized membrane plate', 'Homogenized
    membrane plate','Location','NorthWest')
188 axis([55 85 -10 500])
189 values_5 = num2str(round(med_5min_press,2)');
190 values_6 = num2str(round(med_5min_homo,2)');
191 txt_5 = cellstr(values_5);
192 txt_6 = cellstr(values_6);
193 text(temp+0.5, med_5min_press+8, txt_5),text(temp-0.5,
    med_5min_homo+22, txt_6);
194 print('U:\Diplomarbeit Latex\Figs\10min_UV_homo','-depsc'
    )
195 print('U:\Bonding Technologies\Diplomarbeit\zweite
    Teilpräsentation\10min_UV_homo','-djpeg')
```

2. R Code

```
#Read data from csv-files
results_10min = read.table("C:\\Users\\egleichweit\\Desktop
    \\Data Diplomarbeit\\10_min_pressure_time.csv", sep = ";"
    , header = TRUE, stringsAsFactors = FALSE)
results_5min = read.table(file = "C:\\Users\\egleichweit\\
    Desktop\\Data Diplomarbeit\\5_min_pressure_time.csv", sep
     = ";", header = TRUE, stringsAsFactors = FALSE)
results_0min_exp = read.table("C:\\Users\\egleichweit\\
    Desktop\\Data Diplomarbeit\\0_min_exposure.csv", sep = ";
    ", header = TRUE, stringsAsFactors = FALSE)

temp = results_10min[,1]
temp_60_deg = temp[1]
temp_65_deg = temp[9]
temp_70_deg = temp[17]
```

```
temp_75_deg = temp[25]
temp_80_deg = temp[33]

b_str_10min = results_10min[,2]
b_str_5min = results_5min[,2]
b_str_0min_exp = results_0min_exp[,2]

#Data separation of 10 min pressure holding time
b_str_10min_60C = b_str_10min[1:8]
b_str_10min_65C = b_str_10min[9:16]
b_str_10min_70C = b_str_10min[17:24]
b_str_10min_75C = b_str_10min[25:32]
b_str_10min_80C = b_str_10min[33:40]

mean_10min_60C = mean(b_str_10min_60C)
mean_10min_65C = mean(b_str_10min_65C)
mean_10min_70C = mean(b_str_10min_70C)
mean_10min_75C = mean(b_str_10min_75C)
mean_10min_80C = mean(b_str_10min_80C)

med_10min_60C = median(b_str_10min_60C)
med_10min_65C = median(b_str_10min_65C)
med_10min_70C = median(b_str_10min_70C)
med_10min_75C = median(b_str_10min_75C)
med_10min_80C = median(b_str_10min_80C)

#Data separation of 5 min pressure holding time (10 min UV/
   ozone exposure)
b_str_5min_60C = b_str_5min[1:10]
b_str_5min_65C = b_str_5min[11:20]
b_str_5min_70C = b_str_5min[21:30]
b_str_5min_75C = b_str_5min[31:40]
b_str_5min_80C = b_str_5min[41:50]

mean_5min_60C = mean(b_str_5min_60C)
```

```
mean_5min_65C = mean(b_str_5min_65C)
mean_5min_70C = mean(b_str_5min_70C)
mean_5min_75C = mean(b_str_5min_75C)
mean_5min_80C = mean(b_str_5min_80C)

med_5min_60C = median(b_str_5min_60C)
med_5min_65C = median(b_str_5min_65C)
med_5min_70C = median(b_str_5min_70C)
med_5min_75C = median(b_str_5min_75C)
med_5min_80C = median(b_str_5min_80C)

#Data separation of 0 min UV/ozone exposure time
b_str_0min_exp_60C = b_str_0min_exp[1:4]
b_str_0min_exp_65C = b_str_0min_exp[5:8]
b_str_0min_exp_70C = b_str_0min_exp[9:12]
b_str_0min_exp_75C = b_str_0min_exp[13:16]
b_str_0min_exp_80C = b_str_0min_exp[17:20]



temp_vec <- c(temp_60_deg,temp_65_deg,temp_70_deg,temp_75_
    deg,temp_80_deg)
med_10min_vec <- c(med_10min_60C,med_10min_65C,med_10min_70C
    ,med_10min_75C,med_10min_80C)
med_5min_vec <- c(med_5min_60C, med_5min_65C, med_5min_70C,
    med_5min_75C, med_5min_80C)
med_mat_10_min <- matrix(c(temp_vec,med_10min_vec),5)
med_mat_5_min <- matrix(c(temp_vec,med_5min_vec), 5)

#Test normal distribution of data for pressure holding time
    of 10 min
shapiro.test(b_str_10min_80C)
#p-value = 0,493 > 0,05 normally distributed
#alpha =  5%
shapiro.test(b_str_10min_75C)
#p-value = 0,3392 > 0,05 normally distributed
```

```
shapiro.test(b_str_10min_70C)
#p-value = 0,9748 > 0,05 normally distributed
shapiro.test(b_str_10min_65C)
#p-value = 0,6699 > 0,05 normally distributed
shapiro.test(b_str_10min_60C)
#p-value = 0,9024 > 0,05 normally distributed

#Test normal distribution of pressure holding time of 5 min
   (10 min UV/ozone exposure)
shapiro.test(b_str_5min_80C)
#p-value = 0,05147 > 0,05 normally distributed
shapiro.test(b_str_5min_75C)
#p-value = 0,806 > 0,05 normally distributed
shapiro.test(b_str_5min_70C)
#p-value = 0,7543 > 0,05 normally distributed
shapiro.test(b_str_5min_65C)
#p-value = 0,0003168 < 0,05 NOT normally distributed
shapiro.test(b_str_5min_60C)
#p-value = 1,754*10^-6 < 0,05 NOT normally distributed

#Test normal distribution for 0 min UV/ozone (5 min pressure
    holding time)
shapiro.test(b_str_0min_exp_60C)
#Error: always the same value (crack length = max.)
shapiro.test(b_str_0min_exp_65C)
#Error: always the same value (crack length = max.)
shapiro.test(b_str_0min_exp_70C)
#p-value = 0,1753 > 0,05 normally distributed
shapiro.test(b_str_0min_exp_75C)
#p-value = 0,7517 > 0,05 normally distributed
shapiro.test(b_str_0min_exp_80C)
#p-value = 0,2163 > 0,05 normally distributed

#T-test on significane of 0 and 10 min UV/ozone exposure (5
   min pressure holding time)
```

```
var.test(b_str_0min_exp_70C, b_str_5min_70C, alternative = "
    two.sided")
t.test(b_str_0min_exp_70C, b_str_5min_70C, alternative = "
    two.sided", var.equal=FALSE, paired=FALSE)

var.test(b_str_0min_exp_75C, b_str_5min_75C, alternative = "
    two.sided")
t.test(b_str_0min_exp_75C, b_str_5min_75C, alternative = "
    two.sided", var.equal=TRUE, paired=FALSE)

var.test(b_str_0min_exp_80C, b_str_5min_80C, alternative = "
    two.sided")
t.test(b_str_0min_exp_80C, b_str_5min_80C, alternative = "
    two.sided", var.equal=FALSE, paired=FALSE)
#Significantly different

#T-Test on significance of 5 and 10min pressure holding time
var.test(b_str_10min_70C, b_str_5min_70C, alternative = "two
    .sided")
t.test(b_str_10min_70C, b_str_5min_70C, alternative = "two.
    sided", var.equal=TRUE, paired=F)

var.test(b_str_10min_75C, b_str_5min_75C, alternative = "two
    .sided")
t.test(b_str_10min_75C, b_str_5min_75C, alternative = "two.
    sided", var.equal=TRUE, paired=F)

var.test(b_str_10min_80C, b_str_5min_80C, alternative = "two
    .sided")
t.test(b_str_10min_80C, b_str_5min_80C, alternative = "two.
    sided", var.equal=FALSE, paired=F)
```

```
#Comparison between homogenized and non-homogenized membrane
    plate
#0 min UV/ozone exposure and 10 min UV/ozone exposure
#both: 5 min pressure holding time

#Read in files of results of homogenized membrane plate
results_5min_hom = read.table("C:\\Users\\egleichweit\\
   Desktop\\Data Diplomarbeit\\5_min_pressure_time_
   homogenisiert_1538MPa.csv", sep = ";", header = TRUE,
   stringsAsFactors = FALSE)
results_0min_hom = read.table("C:\\Users\\egleichweit\\
   Desktop\\Data Diplomarbeit\\0_min_exposure_homogenisiert_
   1538MPa.csv", sep = ";", header = TRUE, stringsAsFactors
   = FALSE)

b_str_5min_hom = results_5min_hom[,2]

b_str_0min_hom = results_0min_hom[,2]

b_str_5min_hom_60 = b_str_5min_hom[1:10]
b_str_5min_hom_65 = b_str_5min_hom[11:20]
b_str_5min_hom_70 = b_str_5min_hom[21:30]
b_str_5min_hom_75 = b_str_5min_hom[31:40]
b_str_5min_hom_80 = b_str_5min_hom[41:50]

b_str_0min_hom_60 = b_str_0min_hom[1:4]
b_str_0min_hom_65 = b_str_0min_hom[5:8]
b_str_0min_hom_70 = b_str_0min_hom[9:12]
b_str_0min_hom_75 = b_str_0min_hom[13:16]
b_str_0min_hom_80 = b_str_0min_hom[17:20]

shapiro.test(b_str_5min_hom_60)
#p-value < 0,05 not normally distributed
shapiro.test(b_str_5min_hom_65)
```

```
#p-value < 0,05 not normally distributed
shapiro.test(b_str_5min_hom_70)
#p-value > 0,05
shapiro.test(b_str_5min_hom_75)
#p-value > 0,05
shapiro.test(b_str_5min_hom_80)
#p-value > 0,05

shapiro.test(b_str_5min_60C)
#p-value < 0,05 not normally distributed
shapiro.test(b_str_5min_65C)
#p-value < 0,05 not normally distributed
shapiro.test(b_str_5min_70C)
#p-value > 0,05
shapiro.test(b_str_5min_75C)
#p-value > 0,05
shapiro.test(b_str_5min_80C)
#p-value > 0,05

shapiro.test(b_str_0min_hom_60)
#all values are the same
shapiro.test(b_str_0min_hom_65)
#all values are the same
shapiro.test(b_str_0min_hom_70)
#p-value > 0,05
shapiro.test(b_str_0min_hom_75)
#p-value > 0,05
shapiro.test(b_str_0min_hom_80)
#p-value > 0,05

shapiro.test(b_str_0min_exp_60C)
#all values are the same
shapiro.test(b_str_0min_exp_65C)
#all values are the same
shapiro.test(b_str_0min_exp_70C)
```

```
#p-value > 0,05
shapiro.test(b_str_0min_exp_75C)
#p-value > 0,05
shapiro.test(b_str_0min_exp_80C)
#p-value > 0,05

#60ÂřC und 65ÂřC: Data are not normally distributed
var.test(b_str_5min_hom_70, b_str_5min_70C, alternative = "
    two.sided")
t.test(b_str_5min_hom_70, b_str_5min_70C, alternative = "two
    .sided", var.equal=FALSE, paired=F)
# > 0,05
var.test(b_str_5min_hom_75, b_str_5min_75C, alternative = "
    two.sided")
t.test(b_str_5min_hom_75, b_str_5min_75C, alternative = "two
    .sided", var.equal=FALSE, paired=F)
# < 0,05
var.test(b_str_5min_hom_80, b_str_5min_80C, alternative = "
    two.sided")
t.test(b_str_5min_hom_80, b_str_5min_80C, alternative = "two
    .sided", var.equal=FALSE, paired=F)
# < 0,05

#FÃijr 60ÂřC und 65ÂřC sind alle Werte gleich
var.test(b_str_0min_hom_70, b_str_0min_exp_70C, alternative
    = "two.sided")
t.test(b_str_0min_hom_70, b_str_0min_exp_70C, alternative =
    "two.sided", var.equal=FALSE, paired=F)
# > 0,05
var.test(b_str_0min_hom_75, b_str_0min_exp_75C, alternative
    = "two.sided")
t.test(b_str_0min_hom_75, b_str_0min_exp_75C, alternative =
    "two.sided", var.equal=TRUE, paired=F)
# > 0,05
var.test(b_str_0min_hom_80, b_str_0min_exp_80C, alternative
```

```
   = "two.sided")
t.test(b_str_0min_hom_80, b_str_0min_exp_80C, alternative =
   "two.sided", var.equal=TRUE, paired=F)
# > 0,05
```